Journal of Theoretical Biology 310 (2012) 55–79

Contents lists available at SciVerse ScienceDirect

Journal of Theoretical Biology

journal homepage: www.elsevier.com/locate/yjtbi

Intermittent control with ankle, hip, and mixed strategies during quiet standing: A theoretical proposal based on a double inverted pendulum model

Yasuyuki Suzuki [a], Taishin Nomura [a,*], Maura Casadio [b], Pietro Morasso [c]

[a] Graduate School of Engineering Science, Osaka University, Toyonaka, Osaka 5608531, Japan
[b] University of Genoa, Genoa, Italy
[c] Fondazione Istituto Italiano di Tecnologia, RBCS Department, Genoa, Italy

HIGHLIGHTS

- Human upright posture is modeled by a double inverted pendulum.
- Stabilization can hardly be achieved by a continuous delay feedback control.
- We propose an intermittent control model of the double inverted pendulum.
- The model can achieve robust and flexible stability despite a large feedback delay.
- Distinct coordinated motor patterns during postural sway are emerged in the model.

ARTICLE INFO

Article history:
Received 21 May 2012
Received in revised form
13 June 2012
Accepted 14 June 2012
Available online 23 June 2012

Keywords:
Posture control
Intermittent control
Discontinuous control
Hip strategy
Motor coordination

ABSTRACT

Human upright posture, as a mechanical system, is characterized by an instability of saddle type, involving both stable and unstable dynamic modes. The brain stabilizes such system by generating active joint torques, according to a time-delayed neural feedback control. What is still unsolved is a clear understanding of the control strategies and the control mechanisms that are used by the central nervous system in order to stabilize the unstable posture in a robust way while maintaining flexibility. Most studies in this direction have been limited to the single inverted pendulum model, which is useful for formalizing fundamental mechanical aspects but insufficient for addressing more general issues concerning neural control strategies. Here we consider a double inverted pendulum model in the sagittal plane with small passive viscoelasticity at the ankle and hip joints. Despite difficulties in stabilizing the double pendulum model in the presence of the large feedback delay, we show that robust and flexible stabilization of the upright posture can be established by an intermittent control mechanism that achieves the goal of stabilizing the body posture according to a "divide and conquer strategy", which switches among different controllers in different parts of the state space of the double inverted pendulum. Remarkably, it is shown that a global, robust stability is achieved even if the individual controllers are unstable and the information exploited for switching from one controller to another is severely delayed, as it happens in biological reality. Moreover, the intermittent controller can automatically resolve coordination among multiple active torques associated with the muscle synergy, leading to the emergence of distinct temporally coordinated active torque patterns, referred to as the intermittent ankle, hip, and mixed strategies during quiet standing, depending on the passive elasticity at the hip joint.

1. Introduction

Human upright posture in the sagittal plane during quiet standing is unstable due to the gravitational toppling torque that is greater than the restoring torque generated by the passive viscoelasticity of the joints. The unstable upright equilibrium is saddle-type, involving both stable and unstable modes. In the state-space representation of the system, those two modes correspond to stable and unstable manifolds, i.e., regions where the postural state transits close to an equilibrium point and regions where it falls away from the upright position, respectively (Morasso and Sanguineti, 2002). The unstable posture thus needs to be stabilized by neural feedback control generating active joint torques, with the problem that the neural transmission delay in

* Corresponding author. Tel.: +81 6 6850 6532; fax: +81 6 6850 6534.
E-mail address: taishin@bpe.es.osaka-u.ac.jp (T. Nomura).

0022-5193
http://dx.doi.org/10.1016/j.jtbi.2012.06.019

the loop of about 180–200 ms (Peterka, 2002) is itself a source of instability. Unsolved issue until today is to reveal the control strategy of how the central nervous system (CNS) stabilizes the unstable posture in a robust way while maintaining flexibility that allows the body to exhibit measurable postural sway during quiet standing (Prieto et al., 1996).

Bottaro et al. (2008) and Asai et al. (2009) have proposed an intermittent control model that can establish the robust and flexible stability of the upright posture using single inverted pendulum models actuated at the ankle joint. This model alternates between two types of unstable dynamics, as a function of the time-delayed physical state of the body pendulum: (1) one mode is characterized by the fact that the active torque is turned off when the pendulum state is located near the stable manifold of the saddle instability; (2) in the other mode, which operates in the remaining time periods, the state is driven by the delayed feedback controller. It is remarkable that although both modes are unstable "in the large", i.e., if any of them was adopted permanently, their combination with an appropriate "switching function" is stable and robust.

Note that the intermittent control is not the same as the bang-bang control discussed in the past (Collins and De Luca, 1993), although both strategies consider the state-dependent switchings between an open-loop control without the active torque and a closed-loop control with the active torque. The intermittent control claims a role played by the stable manifold of the system along which the body pendulum transiently approaches the upright equilibrium during the open-loop control. While in the bang-bang control, deterministic dynamics of the system with the open-loop control do not play significant roles for stabilizing the upright posture.

Another debate on the neural control strategy during quiet standing argues whether the CNS utilizes continuous feedback control (Masani et al., 2003; Maurer and Peterka, 2005; Van Der Kooij and De Vlugt, 2007; Vette et al., 2010; Kiemel et al., 2011) or discontinuous intermittent feedback control (Eurich and Milton, 1996; Bottaro et al., 2005, 2008; Asai et al., 2009; Milton et al., 2009a; Insperger and Stepan, 2010; Loram et al., 2011; Gawthrop et al., 2011). This debate is also associated with two questions: (1) if the CNS tries to achieve the stability of the upright posture rather than the minimization of the postural sway (Kiemel et al., 2011) and (2) which type of stability is established by the CNS: either rigid asymptotic stability with a small sway size typically with the continuous stiffness control (Winter et al., 1998) or compliant bounded stability with a relatively large sway size with the intermittent control (Bottaro et al., 2008). The argument may be phrased as "brute force" vs. "gentle taps" in the control of unstable plants (Morasso, 2011).

Theoretical studies considering the postural sway driven by endogenous motor noise have suggested that the sway size, particularly the amplitude of slow oscillations, can alter depending on the stability type of the upright equilibrium as well as on the noise intensity (Bottaro et al., 2008; Asai et al., 2009). Asymptotic stability tends to require a large noise to reproduce the measured sway of amplitude about 1 cm, whereas bounded stability explains sway in a deterministic, noiseless manner. Experimental evaluations have suggested small endogenous noise ($\sim$0.4 N m) due to hemodynamics and respiration (Conforto et al., 2001; Schmid et al., 2004), implying compliant stability. Origins of the flexible posture include small passive ankle stiffness insufficient for stabilizing the upright stance (Loram and Lakie, 2002a; Casadio et al., 2005) and "paradoxical" calf muscle movement, i.e., non-spring like muscle behavior with compliant property of Achilles tendon (Loram et al., 2004) during quiet standing. Moreover, the compliant dynamics that characterize healthy subjects can be lost in neurological patients, as in Parkinson's disease, where postural inflexibility is a common finding (Horak et al., 1992; Yamamoto et al., 2011): this determines at the same time a smaller sway size and a higher postural instability in the patients. Such findings suggest that the CNS controls postural flexibility.

On the other hand, some studies have focused on the beneficial aspects of noise, such as noise-induced stabilization by the use of multiplicative noise (Cabrera and Milton, 2002) or parametric excitation as "drift-and-act" control (Milton et al., 2009b), and improvement of sensory detection of the posture by external noise resulting in sway reduction by the stochastic resonance (Priplata et al., 2002).

Despite different stability types, both control models, namely the continuous control models (Van Der Kooij and De Vlugt, 2007) and the intermittent control models (Bottaro et al., 2008; Asai et al., 2009) can provide good reproductions of the human postural sway, leaving open the question which of them is more physiologically plausible. One reason why both types of control models can comparably reproduce the postural sway is that most studies so far assume single inverted pendulum models as the upright body, making the control problem "easy" even in the presence of the large feedback delay. A double inverted pendulum model makes the control problem substantially more difficult and more physiologically plausible. Thus, we expect that theoretical investigation examining which strategy can stabilize the upright posture of the double pendulum model in a better and robust way would lead to a breakthrough in the debate. Suzuki et al. (2011) have shown that continuous proportional and derivative controllers with the feedback delay can hardly stabilize a physiological double inverted pendulum model due to the delay-induced instability. Of course, the control problem becomes easier if large passive ankle and hip stiffness were assumed. However, the large passive stiffness supplemented by the active feedback torques might result in a markedly rigid stability, contradicting the compliant nature of the upright stance. Thus, it is more likely that values of the passive ankle and hip stiffness during quiet stance are smaller than the critical values required for stabilizing the upright stance only by the passive stiffness.

The double pendulum model requires the CNS controller to resolve motor coordination among multiple joints associated with the muscle synergy (Bernstein, 1967). Nashner and McCollum (1985) and subsequent studies (Horak and Nashner, 1986; Runge et al., 1999) have proposed that different postural control strategies adaptively adjust the position of the center of mass (CoM) in response to external impulsive perturbations. One is *the ankle strategy* defined as the CoM repositioning and it is accomplished by moving the whole body as a single inverted pendulum using the active ankle torque. The second is *the hip strategy* defined as the CoM repositioning by moving the body as a double inverted pendulum with anti-phase motion of the ankle and hip joints. Both strategies are apparent in response to external mechanical perturbations, but are not so clear during quiet standing. Several recent studies, however, have shown that hip joint motion during quiet standing is not small but as large as or even larger than the ankle joint motion. Moreover, hip motion is coordinated with the ankle motion, suggesting existence of the hip strategy even during quiet standing (Aramaki et al., 2001; Alexandrov et al., 2005; Creath et al., 2005; Hsu et al., 2007; Pinter et al., 2008; Sasagawa et al., 2009). Contribution of the ankle and hip strategies to stabilizing the quiet upright posture might depend on the passive hip stiffness. If it is large so that the body can be regarded as the single pendulum, a role played by the active hip torque could be small, leading to the ankle strategy as studied by the single inverted pendulum. On the other hand, a small passive hip stiffness may or may not require the active hip torque, possibly inducing the hip strategy. A technical but not irrelevant problem

that complicates the experimental analysis of postural sway in terms of a double-pendulum model is the estimation of the relative contribution of ankle/hip strategies from force-plate data (Colobert et al., 2006).

Although the double inverted pendulum model of upright standing is a significant advancement with respect to the classical inverted pendulum, from the point of view of biological complexity, it is still a simplification because it ignores a number of additional joints in the legs (the knee), the trunk, the neck and the arms. Multi-link models of this kind have been investigated in recent years in the framework of "anticipatory postural adjustments" and "whole body reaching" (Bouisset and Zattara, 1987; Stapley et al., 1999; Aruin, 2002; Pozzo et al., 2002; Kaminski, 2007; Morasso et al., 2010; Krishnan et al., 2011; Manista and Ahmed, 2012). However, the focus was mainly on synergy formation rather than stabilization and control. Understanding how the standing human body can prepare for action, while maintaining stability in a wide range of situations and tasks, is an ambitious goal for the future but we think that this study sets the necessary groundwork because addressing the stability issue in two dimensions rather than just one is the crucial first step. In particular, this study addresses a number of crucial issues. Is intermittent control superior to the continuous stiffness control for robust and flexible stabilization of the physiological double inverted pendulum model? If intermittent control is indispensable, how should active torques at the ankle and hip be coordinated temporally? How does the neural controller coordinate the control actions? Moreover, how does the coordination depend on the passive hip stiffness that might affect the strategy taken by the CNS?

In Section 2, we define the continuous and the intermittent control models. Preliminary analyses of the continuous models are performed, since we need to characterize stable manifolds of the models for defining the intermittent control strategy. Moreover, we carefully observe dynamics along the stable and unstable manifolds of the model when the active controls are turned off, since those dynamics are key to stabilizing the upright posture. In Section 3, we show that intermittent control can compensate the delay-induced instability and stabilize the double inverted pendulum in a robust way by generating coordinated active torque patterns that change dynamically depending on the passive hip stiffness, referred to as the intermittent ankle, hip, and mixed strategies. Section 4 considers the stochastic dynamics of the intermittent control model driven by noise, showing that the proposed controller generates biologically plausible sway patterns and is also much more energetically efficient than the continuous strategy. In Section 5, we analyze the model's dynamics to understand how the intermittent ankle, hip, and mixed strategies emerge. In particular, we address the issue of how the distinct combination of unstable dynamics exhibited by the open-loop and the closed-loop models, specific to each of three types of the intermittent strategies, can stabilize the overall dynamics. To this end, we analyze the state space and geometry of the stable manifold of the unstable open-loop model and the unstable manifolds of the closed-loop models. We then discuss the results in Section 6.

2. Models and preliminary analyses

2.1. Double inverted pendulum models with and without continuous active feedback control

We consider a double inverted pendulum model during quiet standing in the sagittal plane (Fig. 1). Upper and lower links of the model correspond to the head-arm-trunk (HAT) and the lower extremities, respectively. The distal end of lower link is fixed in the space by a pin joint, corresponding to the ankle joint. The proximal end of lower link and the distal end of upper link are connected also by a pin joint, corresponding to the hip joint. The ankle and hip joint angles (θ_a and θ_h) and the body parameters are defined in Fig. 1. The parameter values are listed in Table 1 for an adult with 1.7 m of height and 60 kg of weight based on Colobert et al. (2006).

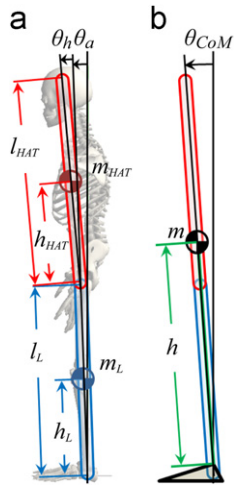

Fig. 1. A double inverted pendulum model. (a) The model consists of upper (HAT) and lower links with ankle and hip joints. See Table 2 for symbols and values of parameters. (b) m represents the total mass of the double pendulum, h the distance from ankle joint to the total center of mass (CoM) of the double pendulum when the hip joint is fully extended.

Since the state variables of the model, i.e., the joint angles $\boldsymbol{\theta}=(\theta_a,\theta_h)^{\mathrm{T}}$ and the corresponding angular velocities $\dot{\boldsymbol{\theta}}$ are small during quiet standing, the second and higher order terms can be neglected, leading to the following linearized equation of motion for the double inverted pendulum model:

$$\mathbf{M}\ddot{\boldsymbol{\theta}}+\mathbf{G}\boldsymbol{\theta}=\mathbf{Q} \tag{1}$$

where $\mathbf{M}$ is the inertia matrix, $\mathbf{G}\boldsymbol{\theta}$ the gravitational toppling torque vector, and $\mathbf{Q}=(\tau_a,\tau_h)^{\mathrm{T}}$ the joint torque vector at the ankle and the hip. The matrices $\mathbf{M}$ and $\mathbf{G}$ are defined in Appendix A.

The joint torques τ_a and τ_h are modeled as the sum of passive torques ($\tau_a^{\mathrm{passive}}$ and $\tau_h^{\mathrm{passive}}$) determined mechanically without feedback delay and active torques (τ_a^{active} and τ_h^{active}) determined by the CNS with feedback delay. The passive ankle and hip torques are modeled as linear torsional viscoelastic elements with passive elastic (K_a and K_h) and viscosity (B_a and B_h) coefficients. We assume that the active torques are generated by linear PD feedback controllers, with proportional (P_a and P_h) and derivative (D_a and D_h) gains for the joint angles and their velocities, conveyed with the feedback delay of Δ seconds. We use such simple neural controllers for the active torques, in agreement with most previous studies of postural stability based on a single inverted pendulum model (Bottaro et al., 2008; Asai et al., 2009; Masani et al., 2003; Maurer and Peterka, 2005; Van Der Kooij and De Vlugt, 2007; Vette et al., 2010). However, we do not think that there is a significant loss of generality, due to the small size of the postural oscillations. For simplicity, we also assume that the desired values of joint angles and velocities are null for both ankle and hip, corresponding to the fully vertical upright posture. The angular velocities at time t are denoted as $\omega_a\equiv d\theta_a(t)/dt$ and $\omega_h\equiv d\theta_h(t)/dt$. Postural variables with the delay Δ are denoted as $\theta_{a\Delta}\equiv\theta_a(t-\Delta)$, $\theta_{h\Delta}\equiv\theta_h(t-\Delta)$, $\omega_{a\Delta}\equiv\omega_a(t-\Delta)$, and $\omega_{h\Delta}\equiv\omega_h(t-\Delta)$. In summary, the passive

Table 1
List of models.

Model name	Description
ODE	Ordinary differential equation
DDE	Delay differential equation with feedback delay time Δ
Off–off model	ODE model with no active torques
On–off model	DDE model with active ankle torque
Off–on model	DDE model with active hip torque
On–on model	DDE model with active ankle and hip torques
ODE on–off model	On–off model with $\Delta=0$ (used only for comparison)
ODE off–on model	Off–on model with $\Delta=0$ (used only for comparison)
ODE on–on model	On–on model with $\Delta=0$ (used only for comparison)
A-ODE model	Approximated ODE of the on–off, the off–on, and the on–on models
A-on–off model	A-ODE model of the on–off model
A-off–on model	A-ODE model of the off–on model
A-on–on model	A-ODE model of the on–on model
(Off–off, on–off, off–on, on–on) model	Intermittent model switching among off–off/on–off/off–on/on–on models
(Off–off, on–off) model	Reduced intermittent model switching between off–off and on–off models
(Off–off, off–on) model	Reduced intermittent model switching between off–off and off–on models
(Off–off, on–on) model	Reduced intermittent model switching between off–off and on–on models

and active torques are formulated as follows:

$$\tau_a^{\text{passive}}(\theta_a,\omega_a) = -K_a\theta_a - B_a\omega_a \tag{2}$$

$$\tau_h^{\text{passive}}(\theta_h,\omega_h) = -K_h\theta_h - B_h\omega_h \tag{3}$$

$$\tau_a^{\text{active}}(\theta_{a\Delta},\omega_{a\Delta}) = -P_a\theta_{a\Delta} - D_a\omega_{a\Delta} \tag{4}$$

$$\tau_h^{\text{active}}(\theta_{h\Delta},\omega_{h\Delta}) = -P_h\theta_{h\Delta} - D_h\omega_{h\Delta} \tag{5}$$

The passive torques are always and continuously acting on the joints, since they are generated by intrinsic mechanical properties, whereas the active torques can be turned on and off by the CNS in the intermittent control paradigm. In particular, the model investigated in this paper considers the following four simple continuous control models of the double inverted pendulum to be alternated during the postural stabilization process: (1) the *off–off model* with no active torques; (2) the *on–off model* with active torque only at the ankle; (3) the *off–on model* with active torque only at the hip; (4) the *on–on model* with active torques on both joints. Fig. 2(a)–(d) shows the corresponding block diagrams of the control models. Specifically, τ_a and τ_h for each control model are defined as follows.

Joint torque of the off–off model (Fig. 2(a)):

$$\begin{pmatrix}\tau_a\\ \tau_h\end{pmatrix} = \begin{pmatrix}\tau_a^{\text{passive}}(\theta_a,\omega_a)\\ \tau_h^{\text{passive}}(\theta_h,\omega_h)\end{pmatrix} = \begin{pmatrix}-K_a\theta_a - B_a\omega_a\\ -K_h\theta_h - B_h\omega_h\end{pmatrix} \equiv \mathbf{T}_{\text{passive}}\begin{pmatrix}\theta_a\\ \theta_h\\ \omega_a\\ \omega_h\end{pmatrix} \tag{6}$$

Joint torque of the on–off model (Fig. 2(b)):

$$\begin{aligned}\begin{pmatrix}\tau_a\\ \tau_h\end{pmatrix} &= \begin{pmatrix}\tau_a^{\text{passive}}(\theta_a,\omega_a)+\tau_a^{\text{active}}(\theta_{a\Delta},\omega_{a\Delta})\\ \tau_h^{\text{passive}}(\theta_h,\omega_h)\end{pmatrix}\\ &= \begin{pmatrix}-K_a\theta_a - B_a\omega_a - P_a\theta_{a\Delta} - D_a\omega_{a\Delta}\\ -K_h\theta_h - B_h\omega_h\end{pmatrix}\\ &\equiv \mathbf{T}_{\text{passive}}\begin{pmatrix}\theta_a\\ \theta_h\\ \omega_a\\ \omega_h\end{pmatrix} + \mathbf{T}_{\text{active}}^{\text{on-off}}\begin{pmatrix}\theta_{a\Delta}\\ \theta_{h\Delta}\\ \omega_{a\Delta}\\ \omega_{h\Delta}\end{pmatrix}\end{aligned} \tag{7}$$

Joint torque of the off–on model (Fig. 2(c)):

$$\begin{aligned}\begin{pmatrix}\tau_a\\ \tau_h\end{pmatrix} &= \begin{pmatrix}\tau_a^{\text{passive}}(\theta_a,\omega_a)\\ \tau_h^{\text{passive}}(\theta_h,\omega_h)+\tau_h^{\text{active}}(\theta_{h\Delta},\omega_{h\Delta})\end{pmatrix}\\ &= \begin{pmatrix}-K_a\theta_a - B_a\omega_a\\ -K_h\theta_h - B_h\omega_h - P_h\theta_{h\Delta} - D_h\omega_{h\Delta}\end{pmatrix}\\ &\equiv \mathbf{T}_{\text{passive}}\begin{pmatrix}\theta_a\\ \theta_h\\ \omega_a\\ \omega_h\end{pmatrix} + \mathbf{T}_{\text{active}}^{\text{off-on}}\begin{pmatrix}\theta_{a\Delta}\\ \theta_{h\Delta}\\ \omega_{a\Delta}\\ \omega_{h\Delta}\end{pmatrix}\end{aligned} \tag{8}$$

Joint torque of the on–on model (Fig. 2(d)):

$$\begin{aligned}\begin{pmatrix}\tau_a\\ \tau_h\end{pmatrix} &= \begin{pmatrix}\tau_a^{\text{passive}}(\theta_a,\omega_a)+\tau_a^{\text{active}}(\theta_{a\Delta},\omega_{a\Delta})\\ \tau_h^{\text{passive}}(\theta_h,\omega_h)+\tau_h^{\text{active}}(\theta_{h\Delta},\omega_{h\Delta})\end{pmatrix}\\ &= \begin{pmatrix}-K_a\theta_a - B_a\omega_a - P_a\theta_{a\Delta} - D_a\omega_{a\Delta}\\ -K_h\theta_h - B_h\omega_h - P_h\theta_{h\Delta} - D_h\omega_{h\Delta}\end{pmatrix}\\ &\equiv \mathbf{T}_{\text{passive}}\begin{pmatrix}\theta_a\\ \theta_h\\ \omega_a\\ \omega_h\end{pmatrix} + \mathbf{T}_{\text{active}}^{\text{on-on}}\begin{pmatrix}\theta_{a\Delta}\\ \theta_{h\Delta}\\ \omega_{a\Delta}\\ \omega_{h\Delta}\end{pmatrix}\end{aligned} \tag{9}$$

The four 2×4 impedance matrices, namely $\mathbf{T}_{\text{passive}}$, $\mathbf{T}_{\text{active}}^{\text{on-off}}$, $\mathbf{T}_{\text{active}}^{\text{off-on}}$, and $\mathbf{T}_{\text{active}}^{\text{on-on}}$, are constant and correspond to the four control models.

2.2. Overview of the intermittent control model of the double inverted pendulum

The intermittent control model proposed in this paper consists of a set of four continuous-time feedback controllers (or model components), with delayed feedback, and a smart switching mechanism that alternates in time between one controller and another in order to achieve a robust, bounded stability. The possible switching patterns are depicted in Fig. 2(e).

We also used reduced intermittent control models that consist of only two model components; one is the off–off model component and the other is either on–off, off–on, or on–on model component. Those reduced models were introduced to specify a model component dominantly responsible for stabilizing the upright posture.

2.3. Parameters for passive viscoelasticity and active feedback control gains

Each continuous control model is characterized by nine parameters: four passive viscoelastic coefficients (K_a,B_a,K_h,B_h), four

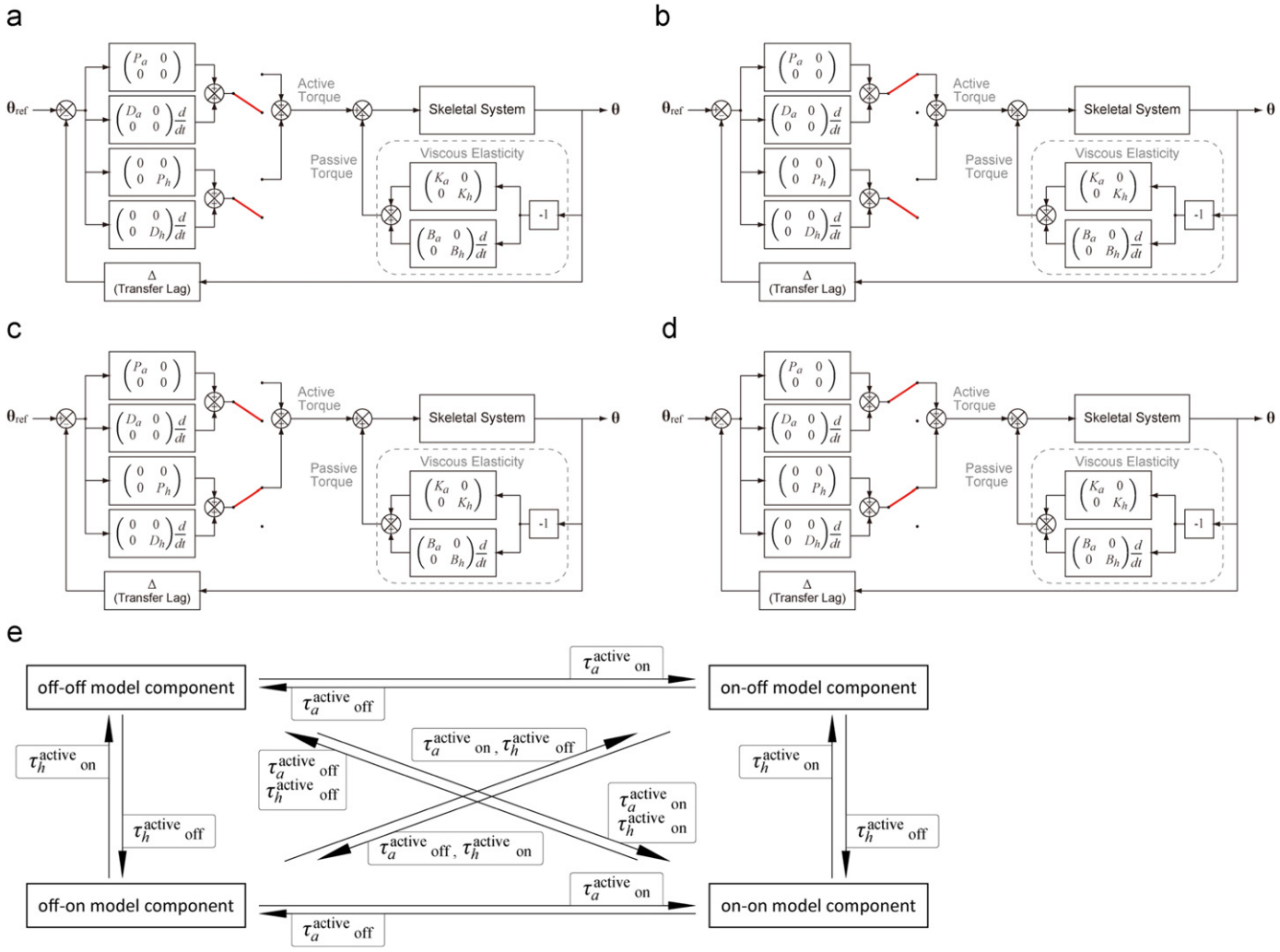

Fig. 2. Block diagrams of the four continuous control models (panels (a), (b), (c), and (d)) of the double inverted pendulum that are used by the intermittent motor controller. Panel (e) shows the possible switching patterns carried out by the controller.

active feedback gains (P_a,D_a,P_h,D_h), and the feedback delay Δ. Table 3 summarizes the values or range of values for those parameters, used in the simulation experiments.

The passive gain parameters were chosen as follows. In particular, the elastic and viscous coefficients of the ankle joint are set and fixed as $K_a/mgh=0.8$ and $B_a=4.0$ N m s/rad for all models, in agreement with specific experimental evaluations (Loram and Lakie, 2002a; Casadio et al., 2005), which show that the single inverted pendulum cannot be stabilized in the upright posture because K_a is smaller than the rate of growth mgh of the gravitational toppling torque. These or similar values were used in most studies of the single inverted pendulums (Bottaro et al., 2008; Asai et al., 2009; Maurer and Peterka, 2005). The feedback delay Δ is fixed at 0.2 s as reported in Peterka (2002).

Unfortunately, there are no experimental evaluations of the passive hip viscoelasticity during quiet standing and thus we analyzed a rather wide range of passive hip elasticity ($K_h/mgh\in[0.3,1.0]$), focusing the attention on three typical values: 0.3, 0.5, and 1.0. The value of B_a is rather small and is set to 4 N m s/rad in agreement with available estimates of ankle impedance. Also for B_h we used a small value (10 N m s/rad), but bigger than B_a in consideration of the fact that the overall cross-sectional area of the muscles acting on the hip joint is greater than ankle muscles. Larger values of B_h would merely reduce the dynamics of the double pendulum, leading to qualitatively similar behavior to the single inverted pendulum. B_h-dependency of the dynamics is discussed briefly in Section 6.

As regards the active gain parameters, we analyzed ranges of values which are listed in Table 3. In particular we focused the attention on the following "typical" values: $P_a/mgh=0.4$, $D_a=10$ N m s/rad, $P_h/mgh=0.6$, and $D_h=10$ N m s/rad. This means that the "typical" intermittent control model is based on the following model components:

$$(P_a/mgh,D_a,P_h/mgh,D_h)=\begin{cases}(0,0,0,0), & \text{the off}-\text{off model}\\ (0.4,10,0,0), & \text{the on}-\text{off model}\\ (0,0,0.6,10), & \text{the off}-\text{on model}\\ (0.4,10,0.6,10), & \text{the on}-\text{on model}\end{cases} \tag{10}$$

These continuous control models act as the model components for the intermittent controller, which switches on and off the different active gains according to a switching strategy that is explained in detail later on. However, we emphasize that such active gain values are all "small", in the sense that each parameter set is far outside the stability region of the corresponding continuous model, as shown in the following. In spite of that, we will demonstrate that a smart switching strategy can achieve dynamic, bounded stability in a robust way.

2.4. Stable and unstable manifolds of the off–off model

In the off–off model, the upright equilibrium posture $(\theta_a,\theta_h,\omega_a,\omega_h)^{\mathrm{T}}=\mathbf{0}$ is unstable for the given passive parameters (K_a,B_a,B_h) and any value of the passive hip stiffness K_h in the analyzed range. This can be confirmed by the stability analysis of Eq. (1), which can be rewritten as the following four-dimensional ordinary differential equation (ODE), taking into account Eq. (6):

$$\frac{d}{dt}\begin{pmatrix}\theta_a\\ \theta_h\\ \omega_a\\ \omega_h\end{pmatrix}=\left\{\begin{pmatrix}\mathbf{0} & \mathbf{I}\\ \mathbf{M}^{-1}\mathbf{-G} & \mathbf{0}\end{pmatrix}+\begin{pmatrix}\mathbf{0}\\ \mathbf{M}^{-1}\mathbf{T}_{\mathrm{passive}}\end{pmatrix}\right\}\begin{pmatrix}\theta_a\\ \theta_h\\ \omega_a\\ \omega_h\end{pmatrix}$$
$$\equiv\mathbf{A}_{\mathrm{passive}}\begin{pmatrix}\theta_a\\ \theta_h\\ \omega_a\\ \omega_h\end{pmatrix} \tag{11}$$

The instability of the off–off model is determined by the fact that one of the four eigenvalues of matrix $\mathbf{A}_{\mathrm{passive}}$ is always positive, as demonstrated by the root-locus analysis (see Fig. C1 in Appendix C). In particular this analysis reveals the saddle-type instability because the four eigenvalues include one positive real (λ_1), one negative real (λ_2), and one pair of complex values with a negative real part (λ_3 and λ_4). Let us denote with $\mathbf{v}_1$, $\mathbf{v}_2$, $\mathbf{v}_3$, and $\mathbf{v}_4$ the corresponding eigenvectors, and let us normalize them as $\|\mathbf{v}_1\|=1$, $\|\mathbf{v}_2\|=1$, and $\|\mathbf{v}_3\|^2+\|\mathbf{v}_4\|^2=1$ just for an analytical convenience.

Such eigenvectors provide the following geometrical interpretations of the dynamics. (1) $\mathbf{v}_1$ spans the one-dimensional unstable manifold on which the state point exhibits unstable monotonic in-phase mode, referred to as the $M^{\mathrm{u,in}}_{\mathrm{off-off}}$-mon, where ankle and hip angles change monotonically falling together in the same directions as illustrated in Fig. 3(a). We refer to this manifold as $E^{\mathrm{u,in}}_{\mathrm{off-off}}$. (2) $\mathbf{v}_2$ spans the one-dimensional stable manifold on which the state point exhibits the stable monotonic in-phase mode, referred to as the $M^{\mathrm{s,in}}_{\mathrm{off-off}}$-mon, where the ankle and hip angles also change monotonically together in the same directions toward the upright position as in Fig. 3(b). We refer to this manifold as $E^{\mathrm{s,in}}_{\mathrm{off-off}}$. (3) $\mathbf{v}_3$ and $\mathbf{v}_4$ span the two-dimensional stable manifold on which the state point exhibits a stable

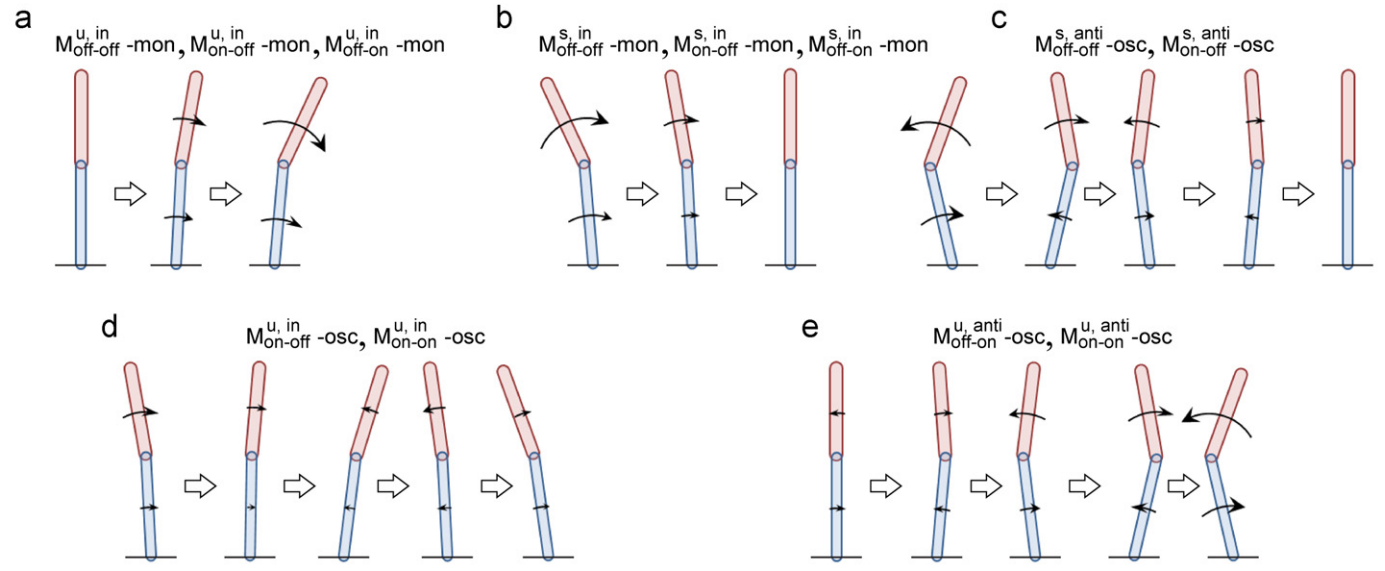

	in-phase			anti-phase	
	monotonic (1-dim)		oscillatory (2-dim)	oscillatory (2-dim)	
	(a) unstable	(b) stable	(d) unstable	(e) unstable	(c) stable
off-off	$M^{\mathrm{u,in}}_{\mathrm{off-off}}$-mon ($E^{\mathrm{u,in}}_{\mathrm{off-off}}$)	$M^{\mathrm{s,in}}_{\mathrm{off-off}}$-mon ($E^{\mathrm{s,in}}_{\mathrm{off-off}}$)			$M^{\mathrm{s,anti}}_{\mathrm{off-off}}$-osc ($E^{\mathrm{s,anti}}_{\mathrm{off-off}}$)
on-off small, medium K_h	$M^{\mathrm{u,in}}_{\mathrm{on-off}}$-mon ($E^{\mathrm{u,in}}_{\mathrm{on-off}}$)	$M^{\mathrm{s,in}}_{\mathrm{on-off}}$-mon ($E^{\mathrm{s,in}}_{\mathrm{on-off}}$)			$M^{\mathrm{s,anti}}_{\mathrm{on-off}}$-osc ($E^{\mathrm{s,anti}}_{\mathrm{on-off}}$)
on-off large K_h			$M^{\mathrm{u,in}}_{\mathrm{on-off}}$-osc ($E^{\mathrm{u,in}}_{\mathrm{on-off}}$)		
off-on	$M^{\mathrm{u,in}}_{\mathrm{off-on}}$-mon ($E^{\mathrm{u,in}}_{\mathrm{off-on}}$)	$M^{\mathrm{s,in}}_{\mathrm{off-on}}$-mon ($E^{\mathrm{s,in}}_{\mathrm{off-on}}$)		$M^{\mathrm{u,anti}}_{\mathrm{off-on}}$-osc ($E^{\mathrm{u,anti}}_{\mathrm{off-on}}$)	
on-on			$M^{\mathrm{u,in}}_{\mathrm{on-on}}$-osc ($E^{\mathrm{u,in}}_{\mathrm{on-on}}$)	$M^{\mathrm{u,anti}}_{\mathrm{on-on}}$-osc ($E^{\mathrm{u,anti}}_{\mathrm{on-on}}$)	

Fig. 3. Modes of the four continuous control models including the off–off model. The upper panels sketch, by means of stick figures, the motion of the double pendulum for various modes determined by the continuous control models: (a) unstable, monotonic in-phase mode, (b) stable, monotonic in-phase mode, (c) stable, oscillatory anti-phase mode, (d) unstable, oscillatory in-phase mode, (e) unstable, oscillatory anti-phase mode. The lower table summarizes the modes exhibited by the four continuous control models for small/medium and large K_h.

oscillatory anti-phase mode, referred to as the $M^{s,anti}_{off-off}$-osc, where the ankle and hip angles oscillate in the opposite directions toward the upright position as in Fig. 3(c). We refer to this manifold as $E^{s,anti}_{off-off}$.

The three modes described above occur in the off–off model for any value of K_h in the designated range. Appendix C provides details of the mode analysis. In summary, a relevant feature of the off–off model, exploited by the intermittent controller, is that it includes a three-dimensional stable manifold: if the state vector happens to be aligned on or near the stable manifold, for some time it will move toward the upright equilibrium state spontaneously, without any active torques provided by the neural controller.

Fig. 4(a) shows the three manifolds and sample trajectories. An initial state point for each trajectory is exactly on one of the manifolds. Thus, the state point developed from the initial state keeps staying on the manifold. Since the off–off model is a linear dynamical system, a trajectory from a state point that is not on any of the three manifolds can be represented uniquely by a linear combination of three trajectories: one on $E^{u,in}_{off-off}$, one on $E^{s,in}_{off-off}$, and the other on $E^{s,anti}_{off-off}$. Thus, the four-dimensional state space E of the off–off model can be represented by the direct sum of the three manifolds as

$$E = E^{u,in}_{off-off} \oplus E^{s,in}_{off-off} \oplus E^{s,anti}_{off-off} \tag{12}$$

Let us represent the state space E using the eigenvectors of the off–off model as the basis, and let us denote with $X=(x_1,x_2,x_3,x_4)$ the corresponding coordinate vector. It is then possible to express the state space with two sets of coordinates, as follows:

$$\begin{pmatrix} x_1 \\ x_2 \\ x_3 \\ x_4 \end{pmatrix} = \mathbf{V}^{-1}_{off-off} \begin{pmatrix} \theta_a \\ \theta_h \\ \omega_a \\ \omega_h \end{pmatrix} \tag{13}$$

where the transformation matrix is defined as $\mathbf{V}_{off-off} = (\mathbf{v}_1,\mathbf{v}_2,\mathbf{v}_3,\mathbf{v}_4)$.

Fig. 4(b) represents a projection of Fig. 4(a) on the x_1–x_2 and x_3–x_4 planes with the coordinate X. The x_1 and x_2 axes represent the one-dimensional unstable and stable manifolds ($E^{u,in}_{off-off}$ and $E^{s,in}_{off-off}$), respectively. The x_3–x_4 plane is the two-dimensional stable manifold $E^{s,anti}_{off-off}$. The three-dimensional space x_2–x_3–x_4, i.e., the subspace of E satisfying $x_1=0$, is the stable manifold of the off–off model, $E^{s,in}_{off-off} \oplus E^{s,anti}_{off-off}$. The three sample trajectories shown in Fig. 4(b) are the same as those in Fig. 4(a), but with the coordinate X. The initial state point on the x_1-axis, which is the unstable manifold $E^{u,in}_{off-off}$, moves away from the upright state monotonically on the x_1-axis with the mode $M^{u,in}_{off-off}$-mon. Similarly, the initial state point on the x_2-axis, which is the stable manifold $E^{s,in}_{off-off}$, moves toward the upright state on the x_2-axis with the mode $M^{s,in}_{off-off}$-mon. Moreover, the initial state point on the x_3–x_4 plane, which is the two-dimensional stable manifold $E^{s,anti}_{off-off}$, moves toward the upright state on the x_3–x_4 plane with oscillating mode $M^{s,anti}_{off-off}$-osc. The intermittent control model considered in this study utilizes the dynamics on the stable manifold $E^{s,in}_{off-off} \oplus E^{s,anti}_{off-off}$ of the off–off model intermittently for stabilizing the upright state of the pendulum.

In the off–off model, the upright state is the intersectional point of the three manifolds, and it is the saddle type unstable equilibrium point around which the vector field exhibits a hyperbolic configuration. Fig. 4(c) shows a sample trajectory from an initial state point close to but not exactly on the three-dimensional stable manifold $E^{s,in}_{off-off} \oplus E^{s,anti}_{off-off}$ of the off–off model. Since the state point is initially located close to the stable manifold, the dynamics of the state point is dominated transiently by the stable manifold, getting closer to the origin for a period of time. See the corresponding hyperbolic trajectory along x_1-axis and transiently converging spiral on the x_3–x_4 plane in Fig. 4(c). The pendulum behaves according to a combination of the two modes, $M^{s,in}_{off-off}$-mon and $M^{s,anti}_{off-off}$-osc.

Eventually, however, the state point moves closer to the unstable manifold $E^{u,in}_{off-off}$, and thus moves away from the origin along $E^{u,in}_{off-off}$ with the mode $M^{u,in}_{off-off}$-mon, leading to the almost

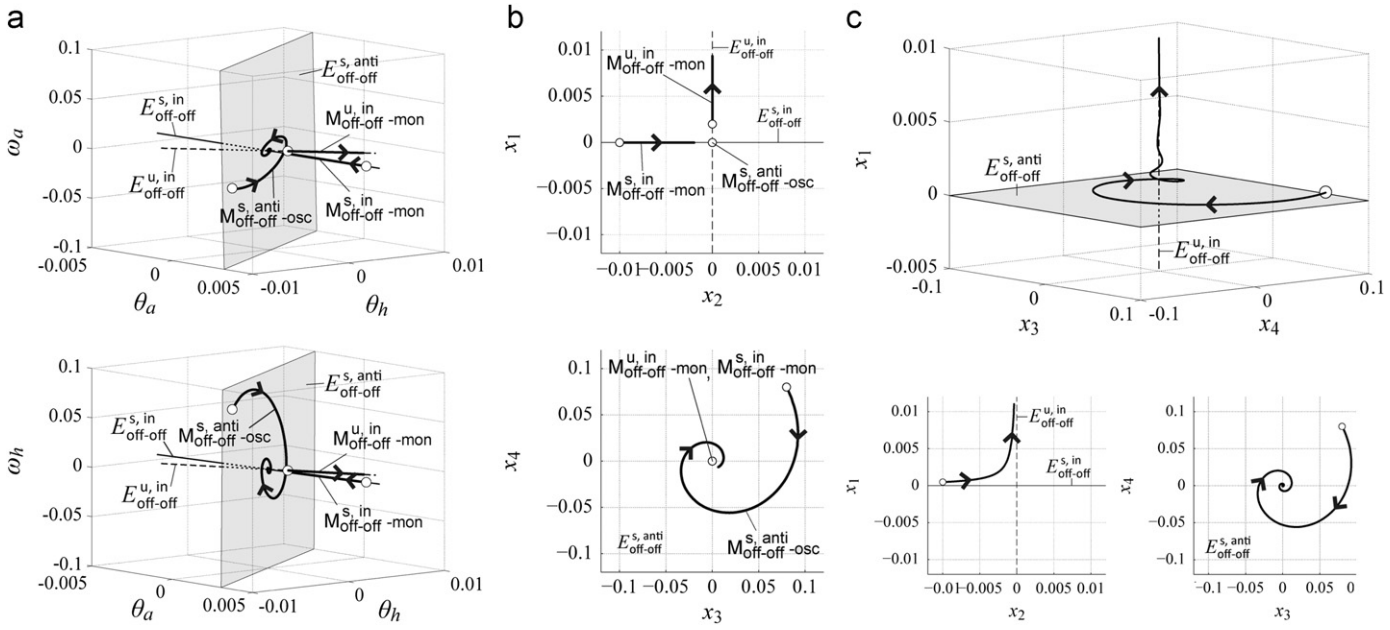

Fig. 4. Manifolds and sample trajectories of the continuous off–off model in the state space E with the standard $\theta-\omega$ coordinate and the coordinate X. In each panel, dashed and solid lines represent the one-dimensional unstable and stable manifolds ($E^{u,in}_{off-off}$ and $E^{s,in}_{off-off}$), respectively. The gray plane is the two dimensional stable manifold ($E^{s,anti}_{off-off}$). ○ markers correspond to initial points of sample state trajectories. (a) Manifolds of the off–off model and sample trajectories in E with $\theta-\omega$ coordinate. Each initial state is located exactly on one of the three manifolds: thus the state point keeps staying on the corresponding manifold. These trajectories correspond to the $M^{u,in}_{off-off}$-mon, $M^{s,in}_{off-off}$-mon, and $M^{s,anti}_{off-off}$-osc modes, illustrated in Fig. 3. (b) Projection of (a) on the two dimensional subspace of E with X coordinates: the x_3–x_4 plane represents the stable manifold of the off–off model. (c) A sample trajectory from an initial state point close to but not exactly on the stable manifold $E^{s,in}_{off-off} \oplus E^{s,anti}_{off-off}$.

monotonic falling. For analyzing the dynamics of the intermittent control model, later in this paper, we represent the transients with transition in the dominant modes described here by using the associated manifolds as follows:

$$E^{\mathrm{u,in}}_{\mathrm{off-off}} \oplus \overline{E^{\mathrm{s,in}}_{\mathrm{off-off}}} \oplus \overline{E^{\mathrm{s,anti}}_{\mathrm{off-off}}} \rightarrow \overline{E^{\mathrm{u,in}}_{\mathrm{off-off}}} \oplus E^{\mathrm{s,in}}_{\mathrm{off-off}} \oplus E^{\mathrm{s,anti}}_{\mathrm{off-off}} \tag{14}$$

where the arrow $\rightarrow$ represents the time evolution, and the upper bar on a manifold means that the dynamics of the model is dominated by the dynamics on that manifold. See Appendix E for determining which manifold dominates the dynamics. Note that, in general, for a state point of a dynamical system with stable and unstable manifolds, the stable manifolds are repulsive and the unstable manifolds are attractive. For this reason, although a state point close to the stable manifold is dominated by it for a transient period of time, the state point gets closer to the unstable manifold dominating the dynamics eventually. The transient dynamics described in Eq. (14) is consistent with this general property.

2.5. Stability and dynamics of the continuous models with active torques

The three continuous models with active torques are characterized by delay differential equations (DDE). Although a detailed analysis of such models is not required for defining the intermittent controller, we need to introduce "approximated" stable manifolds of the DDE models for defining a switching rule among the model components, since they might contribute to stabilizing the standing posture together with the stable manifold of the off–off model. Therefore, for every DDE of the examined range of K_h and (P_a,D_a,P_h,D_h), we briefly illustrate stability and dynamic modes with their associated manifolds. Eq. (1) with the active torque(s) can be rewritten as follows:

$$\begin{aligned}\frac{d}{dt}\begin{pmatrix}\theta_a\\ \theta_h\\ \omega_a\\ \omega_h\end{pmatrix} &= \mathbf{A}_{\mathrm{passive}}\begin{pmatrix}\theta_a\\ \theta_h\\ \omega_a\\ \omega_h\end{pmatrix} + \begin{pmatrix}\mathbf{0}\\ \mathbf{M}^{-1}\mathbf{T}^{i}_{\mathrm{active}}\end{pmatrix}\begin{pmatrix}\theta_{a\Delta}\\ \theta_{h\Delta}\\ \omega_{a\Delta}\\ \omega_{h\Delta}\end{pmatrix}\\ &\equiv \mathbf{A}_{\mathrm{passive}}\begin{pmatrix}\theta_a\\ \theta_h\\ \omega_a\\ \omega_h\end{pmatrix} + \mathbf{A}^{i}_{\mathrm{active}}\begin{pmatrix}\theta_{a\Delta}\\ \theta_{h\Delta}\\ \omega_{a\Delta}\\ \omega_{h\Delta}\end{pmatrix}\end{aligned} \tag{15}$$

where i=on–off, off–on, and on–on. The impedance matrix $\mathbf{T}^{i}_{\mathrm{active}}$ is defined by either Eqs. (7) and (8) or (9). The corresponding eigenequation is

$$\left|\lambda\mathbf{I}-\mathbf{A}_{\mathrm{passive}}-e^{-\lambda\Delta}\mathbf{A}^{i}_{\mathrm{active}}\right| = 0 \tag{16}$$

which has an infinite number of roots, since the DDE of Eq. (15) is an infinite dimensional system. However, for the analysis of the upright posture we are only interested in the four dominant eigenvalues, namely λ^i_1, λ^i_2, λ^i_3, and λ^i_4. We identified them by solving Eq. (16) numerically using the Newton method, as explained in Appendix B. We also obtained the corresponding sets of four eigenvectors, denoted as $\mathbf{v}^i_1$, $\mathbf{v}^i_2$, $\mathbf{v}^i_3$, and $\mathbf{v}^i_4$.

The upright state of the i-th DDE model is stable if real parts of all of four eigenvalues are negative. The stability region of the i-th DDE was analyzed by varying the values of (P_a,D_a,P_h,D_h) and K_h. Such stability regions were also compared with the regions of the corresponding ODE (setting $\Delta=0$ in the equation above) in order to clarify the destabilizing effect of feedback delay. Fig. 5 shows the stability regions of each continuous control model with active torque(s) and that of the corresponding ODE model with $\Delta=0$.

A state of each DDE model at time t is described as a state function defined on the time interval $[t-\Delta,t]$. We denote such state function of the i-th DDE as $x^i([t-\Delta,t])$, and consider the time evolution of the state function in the four dimensional space E, although this is not possible, strictly speaking, since the DDE system evolves in an infinite dimensional space. $x^i([t-\Delta,t])$ may be depicted as a curved segment that moves in space E. We refer to the points $x^i(t)$ and $x^i(t-\Delta)$ as the head and the tail of the curved segment $x^i([t-\Delta,t])$ in E, respectively. To make the DDE models tractable, their dynamics were approximated by those of the corresponding ODE, referred to as approximated ODE model (a-ODE model) or approximated ODE model component (a-ODE model component). The reader should take care distinguishing between the regular ODE models (defined by $\Delta=0$) and the a-ODE models, which are introduced for analyzing the dynamics of DDE models in a finite-dimensional space.

The a-ODE model of the i-th DDE model in the standard coordinate system is defined as follows:

$$\frac{d}{dt}\begin{pmatrix}\theta_a\\ \theta_h\\ \omega_a\\ \omega_h\end{pmatrix} = \mathbf{V}_i\mathbf{\Lambda}_i\mathbf{V}_i^{-1}\begin{pmatrix}\theta_a\\ \theta_h\\ \omega_a\\ \omega_h\end{pmatrix} \tag{17}$$

where the matrix $\mathbf{V}_i=(\mathbf{v}^i_1,\mathbf{v}^i_2,\mathbf{v}^i_3,\mathbf{v}^i_4)$, and $\mathbf{\Lambda}_i$ is the diagonal matrix containing the corresponding eigenvalues λ^i_1, λ^i_2, λ^i_3, and λ^i_4. The a-ODE models with i=on–off, off–on, and on–on define the a-on–off, the a-off–on, and the a-on–on continuous control models, respectively. Since each a-ODE model is a four dimensional dynamical system, a state of the i-th a-ODE model at time t can be represented as a state point in the four dimensional state space E, which approximates the state function $x^i([t-\Delta,t])$. We also define stable and/or unstable manifolds spanned by the eigenvectors for each a-ODE model, and consider them as the approximated manifolds of the corresponding DDE model, which are assumed to capture major aspects of dynamics for the DDE model. This assumption is supported empirically by the simulations examined in the following, but a formal validation is outside the scope of this paper. See Section 6 for related arguments.

2.5.1. Stability, modes, and manifolds of the on–off model

For each examined value of K_h, stability of the on–off model is determined only by P_a and D_a, since $P_h=D_h=0$. Fig. 5(a) shows the stability regions of the on–off model in the $(P_a/mgh,D_a)$-plane for small $(K_h/mgh=0.3)$, medium $(K_h/mgh=0.5)$, and large $(K_h/mgh=1.0)$ values of the passive hip stiffness. For $K_h/mgh=0.3$, there is no stability region for both the DDE and ODE models. For $K_h/mgh=0.5$ and 1.0, the ODE model has rectangular stability regions in the $(P_a/mgh,D_a)$-plane, whereas the DDE models have irregular stability regions, contained in the corresponding rectangle and with quite smaller areas. See also Fig. C1 in Appendix C for the root loci of the four dominant eigenvalues of the on–off model as a function of K_h, where one can confirm that the root loci have two critical values of K_h. That is, as K_h increases, one real eigenvalue changes its sign from negative to positive at $K_h\sim0.5836$, and then one pair of complex eigenvalues appears at $K_h\sim0.5878$. Thus, the dynamics of the on–off model changes qualitatively roughly around $K_h\sim0.58$. For this reason, we consider $K_h=1.0>0.58$ as large, and K_h=0.3 and K_h=0.5 as small or medium.

The state space E of the unstable a-on–off model with small and medium K_h can be represented as

$$E = E^{\mathrm{u,in}}_{\mathrm{on-off}} \oplus E^{\mathrm{s,in}}_{\mathrm{on-off}} \oplus E^{\mathrm{s,anti}}_{\mathrm{on-off}} \tag{18}$$

where $E^{\mathrm{u,in}}_{\mathrm{on-off}}$, $E^{\mathrm{s,in}}_{\mathrm{on-off}}$, and $E^{\mathrm{s,anti}}_{\mathrm{on-off}}$ are associated, respectively, with the unstable monotonic in-phase mode $M^{\mathrm{u,in}}_{\mathrm{on-off}}$-mon (Fig. 3(a)), the stable monotonic in-phase mode $M^{\mathrm{s,in}}_{\mathrm{on-off}}$-mon (Fig. 3(b)), and the stable oscillatory anti-phase mode $M^{\mathrm{s,anti}}_{\mathrm{on-off}}$-osc (Fig. 3(c)). This

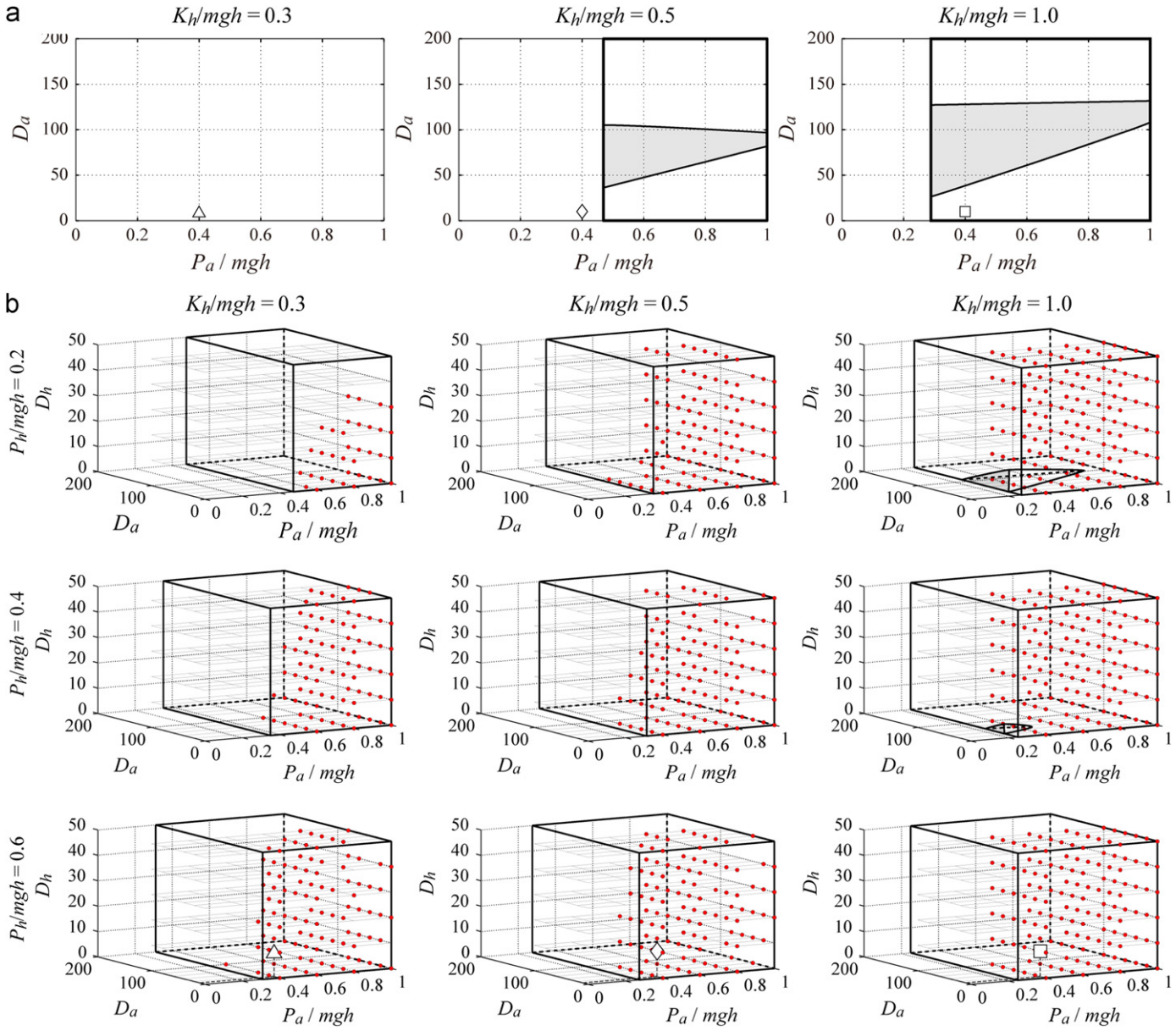

Fig. 5. Intrinsic stability regions of the three continuous control models: on–off (panel a); on–on (panel b); no panel is shown for the off–on since this model, even for the case with $\Delta = 0$, is stable for no combination of control parameters. The following parameters are fixed for all models: $K_a/mgh = 0.8$, B_a=4 N m s/rad, and B_h=10 N m s/rad; the other parameters K_h and (P_a, D_a, P_h, D_h) are sampled in their ranges. (a) Stability region (gray area) of the on–off model with $\Delta = 0.2$ s. The thick line rectangular area represents the stability region of the same model without feedback delay ($\Delta = 0$). Markers △, ◇, and □ indicate the parameter points of $(P_a/mgh, D_a) = (0.4, 10)$ for $K_h/mgh = 0.3$, 0.5, and 1.0, respectively. (b) Stability region of the on–on model in the $(P_a/mgh, D_a, D_h)$-space. Left, middle, and right columns are for cases with small ($K_h/mgh = 0.3$), medium ($K_h/mgh = 0.5$), and large ($K_h/mgh = 1.0$) passive hip stiffness. Top, second, and third rows are for cases with $P_h/mgh = 0.2$, $P_h/mgh = 0.4$, and $P_h/mgh = 0.6$. In each panel, thick line cubic represents the stability region of the on–on model without delay. Parameter spaces only for the large K_h ($K_h/mgh = 1.0$) with small P_h ($P_h/mgh = 0.2$ or 0.4) have the stability region for the on–on model with delay $\Delta = 0.2$ s. Markers △, ◇, and □ indicate the parameter points of $(P_a/mgh, D_a, P_h/mgh, D_h) = (0.4, 10, 0.6, 10)$ for $K_h/mgh = 0.3$, 0.5, and 1.0, respectively. A number of red points in the $(P_a/mgh, D_a, D_h)$-space for different sets of $(K_h/mgh, P_h/mgh)$ in (b) indicate that the upright state of the intermittent control model was stable for each of those points, implying the robust stability of the intermittent control model against the changes in the active gain parameters.

means that the dynamics of the on–off model with small and medium K_h are qualitatively the same as those of the off–off model. For large values of K_h, the stable and unstable monotonic in-phase modes collide and disappear, and the unstable oscillatory in-phase mode $M^{u,in}_{on-off}$-osc (Fig. 3(d)) associated with two-dimensional manifold $E^{u,in}_{on-off}$ appears. Thus the state space E of the a-on–off model with large K_h can be represented as

$$E = E^{u,in}_{on-off} \oplus E^{s,anti}_{on-off} \tag{19}$$

2.5.2. Stability, modes, and manifolds of the off–on model

Stability of the off–on model is determined only by P_h and D_h, since $P_a = D_a = 0$. The analysis shows that there is no stability region in the examined range of (P_h, D_h), regardless of the value of K_h for the models both with delay and without delay. That is, the upright state of the off–on model can never be stabilized for any values of (P_h, D_h) and K_h. Despite this fact, in the next section we show that the upright state of the reduced intermittent control model switching between the off–on and the off–off model components can be stabilized. See also Fig. C1 in Appendix C for

the root loci of the four dominant eigenvalues of the off–on model as the function of K_h.

The state space E of the unstable a-off–on model with small, medium, and large values of K_h can be represented commonly as follows:

$$E = E^{\mathrm{u,in}}_{\mathrm{off-on}} \oplus E^{\mathrm{s,in}}_{\mathrm{off-on}} \oplus E^{\mathrm{u,anti}}_{\mathrm{off-on}} \tag{20}$$

where $E^{\mathrm{u,in}}_{\mathrm{off-on}}$, $E^{\mathrm{s,in}}_{\mathrm{off-on}}$, and $E^{\mathrm{u,anti}}_{\mathrm{off-on}}$ are associated with, respectively, the unstable monotonic in-phase mode $M^{\mathrm{u,in}}_{\mathrm{off-on}}$-mon (Fig. 3(a)), the stable monotonic in-phase mode $M^{\mathrm{s,in}}_{\mathrm{off-on}}$-mon (Fig. 3(b)), and the unstable oscillatory anti-phase $M^{\mathrm{u,anti}}_{\mathrm{off-on}}$-osc (Fig. 3(e)). This means that the off–off and the off–on models share qualitatively the same monotonic in-phase modes.

2.5.3. Stability, modes, and manifolds of the on–on model

Stability of the on–on model is determined by the set of active feedback gains (P_a,D_a,P_h,D_h) for the ankle and hip joints. Fig. 5(b) shows the stability region of the on–on model for particular values of P_h/mgh (0.2, 0.4, and 0.6) in the (P_a/mgh,D_a,D_h)-space. Simulations and theoretical analysis confirm that the stability region of the on–on model with $\Delta = 0$ is large parallelepiped, and it becomes larger as K_h and P_h increase. In comparison, the size of stability regions for the DDE models is quite narrow due to the delay-induced instability. See also Fig. C1 in Appendix C for the root loci of the four dominant eigenvalues of the on–on model as the function of K_h.

The state space E of the unstable a-on–on model with small, medium, and large values of K_h can be represented commonly as follows:

$$E = E^{\mathrm{u,in}}_{\mathrm{on-on}} \oplus E^{\mathrm{u,anti}}_{\mathrm{on-on}} \tag{21}$$

where $E^{\mathrm{u,in}}_{\mathrm{on-on}}$ and $E^{\mathrm{u,anti}}_{\mathrm{on-on}}$ are associated, respectively, with the unstable oscillatory in-phase mode $M^{\mathrm{u,in}}_{\mathrm{on-on}}$-osc (Fig. 3(d)) and the unstable oscillatory anti-phase mode $M^{\mathrm{u,anti}}_{\mathrm{on-on}}$-osc (Fig. 3(e)). The unstable in-phase and anti-phase mode of the on–on model are qualitatively the same as that of the on–off model with large K_h and that of the off–on model, respectively.

2.6. The delayed state-dependent switching rule among model components

We can now define the state-dependent "smart" switching rule among the previously analyzed control model components, which is the core of the proposed intermittent control model. The switching rule uses $x(t-\Delta)$, which is the state of the intermittent control model, i.e., a tail of the state function $x^i([t-\Delta,t])$ for each of three DDE model components or the past state point $x(t-\Delta)$ for the off–off model component governing the system at time t. This rule defines how the brain selects a model component for temporarily driving the pendulum in the direction of the desired equilibrium state. The challenge, of course, is that the CNS must take this decision on the basis of delayed sensory feedback information $x(t-\Delta)$ about the physical state of the pendulum. Considering that $x(t-\Delta)$ is a point in the four-dimensional space E, we define the following three conditions for the intermittent control model that utilizes the four continuous model components (Fig. 2(e)):

- As long as $x(t-\Delta)$ is located in the "neighborhood" of the stable manifold $E^{\mathrm{s,in}}_{\mathrm{off-off}} \oplus E^{\mathrm{s,anti}}_{\mathrm{off-off}}$ of the off–off model, the system is continuously governed by the off–off model component, i.e., both active torques are deactivated. If $x(t-\Delta)$ newly enters into such neighborhood, the intermittent controller switches the model component governing the system to the off–off model.
- As long as $x(t-\Delta)$ is located in the neighborhood of the stable manifold of the a-on–off model ($E^{\mathrm{s,in}}_{\mathrm{on-off}} \oplus E^{\mathrm{s,anti}}_{\mathrm{on-off}}$ or $E^{\mathrm{s,anti}}_{\mathrm{on-off}}$ of the on–off model) but not in the neighborhood of the stable manifold of the off–off model, the system is continuously governed by the on–off model component. If $x(t-\Delta)$ newly enters into the neighborhood of the stable manifold of the a-on–off model, but remains outside the stable manifold of the off–off model, the model component governing the system is switched to the on–off model. This means that, if $x(t-\Delta)$ is in the intersection of the neighborhood of the stable manifold of the off–off model and that of the a-on–off model, the off–off model is used preferably to the on–off model.
- If $x(t-\Delta)$ is located neither in the neighborhood of the stable manifold of the off–off model nor in that of the on–off model at time t, the system is governed by either the on–off, the off–on or the on–on model component, according to a rule which is defined below.

For the definitions of the neighborhoods of the stable manifolds, see Appendix D. In our modeling, we did not use the stable manifold $E^{\mathrm{s,in}}_{\mathrm{off-on}}$ of the off–on model. This is because $E^{\mathrm{s,in}}_{\mathrm{off-on}}$ is one-dimensional space, and practically, $x(t-\Delta)$ can hardly enter the neighborhood of $E^{\mathrm{s,in}}_{\mathrm{off-on}}$. Note that the off–off model is selected only if $x(t-\Delta)$ is in the neighborhood of its stable manifold. However, the on–off model is selected both for utilizing its stable manifold if $x(t-\Delta)$ is in the neighborhood of the stable manifold and for utilizing its unstable dynamics otherwise.

If $x(t-\Delta)$ is located neither in the neighborhood of the stable manifold of the off–off model nor in that of the on–off model, the rule for selecting a model component governing the system at time t is defined as follows. The aim of the control under this situation is to attract the state of the system (the head of the state function) back to the stable manifold of the off–off model component rather than to the nominal equilibrium state. This can be achieved by the use of *unstable dynamics* of the on–off, the off–on, and the on–on model components. In particular, dynamics dominated by any of *unstable oscillatory modes* can achieve this, because the state of the system spiralling around the nominal equilibrium point inevitably gets across the stable manifold of the off–off model component. The point is to choose the best alternative and we did so by evaluating the four dimensional change rate vector at the tail $x(t-\Delta)$ in E for each model component. By using Eq. (15) the change rate vector at $x(t-\Delta)$ in the standard coordinate system can be expressed as follows:

$$\frac{d}{dt}\begin{pmatrix}\theta_{a\Delta}\\ \theta_{h\Delta}\\ \omega_{a\Delta}\\ \omega_{h\Delta}\end{pmatrix} = \mathbf{A}_{\mathrm{passive}}\begin{pmatrix}\theta_{a\Delta}\\ \theta_{h\Delta}\\ \omega_{a\Delta}\\ \omega_{h\Delta}\end{pmatrix} + \mathbf{A}^{i}_{\mathrm{active}}\begin{pmatrix}\theta_{a2\Delta}\\ \theta_{h2\Delta}\\ \omega_{a2\Delta}\\ \omega_{h2\Delta}\end{pmatrix} \tag{22}$$

However, calculating the right-hand-side of this equation requires the delayed physical state of the pendulum at the past time $t-2\Delta$. Since we consider that only the physical state of the pendulum at the past time $t-\Delta$ is available for the CNS at time t, we evaluated the approximated change rate vector at $x(t-\Delta)$ in the standard coordinate as

$$\frac{d}{dt}\begin{pmatrix}\theta_{a\Delta}\\ \theta_{h\Delta}\\ \omega_{a\Delta}\\ \omega_{h\Delta}\end{pmatrix} = \mathbf{V}_i\mathbf{\Lambda}_i\mathbf{V}_i^{-1}\begin{pmatrix}\theta_{a\Delta}\\ \theta_{h\Delta}\\ \omega_{a\Delta}\\ \omega_{h\Delta}\end{pmatrix} \tag{23}$$

using the i-th a-ODE for the i-th DDE model. We propose that, at every time instant t, the CNS selects the model component whose approximated change rate vector $\tilde{r}(t-\Delta)$ evaluated at $x(t-\Delta)$ in E is the one which most quickly directed to the stable manifold of the off–off model. To select the component, we calculated the direction cosine $q^i(t)$ (i=on–off, off–on, and on–on) between each change rate vector of the three model components and a vector in

the direction of the perpendicular line of the stable manifold of the off–off model terminated at the point $x(t-\Delta)$ in E. The latter vector, denoted as $n(t-\Delta)$, can be represented simply as $(x_1,0,0,0)^{\mathrm{T}}$ in the coordinate X, since the three dimensional subspace of E satisfying $x_1=0$ is the stable manifold of the off–off model. The index $q^i(t)$ is defined as follows in the coordinate X:

$$q^i(t)=\frac{n(t-\Delta)\cdot\tilde{r}(t-\Delta)}{\|n(t-\Delta)\|\|\tilde{r}(t-\Delta)\|} \tag{24}$$

The approximated change rate vector $\tilde{r}(t-\Delta)$ in Eq. (24) in the coordinate X was calculated from Eq. (23) using the coordinate transformation matrix $\mathbf{V}_{\mathrm{off-off}}$. If the value of $q_i(t)$ at time t is the closest to -1 for a specific i-th model component, the change rate vector of the corresponding model component directs the most to the stable manifold of the off–off model than those of the others. That is, the use of i-th model component at time t is the locally best selection to pull the state of the system toward the stable manifold of the off–off model. Thus, i-th DDE model component is selected to govern dynamics of the system. Note that the use of the coordinate X for calculating Eq. (24) is optional, and it is just for computational convenience.

The delayed-state-dependent switching rules for the reduced intermittent control models with two model components are basically the same as defined above for the intermittent control model composed of four model components. For example, for the off–off/off–on reduced model, only the first item of the switching conditions is employed without considering the use of the on–off and the on–on model components, i.e., the off–on controller is selected whenever the first condition for the use of the off–off model is not satisfied.

3. Intermittent control stabilizes the double inverted pendulum

We show here that the upright state of the double inverted pendulum can be stabilized by the proposed intermittent feedback controller, in spite of the fact that none of the four continuous model components alternated in time is stable in the target posture. Fig. 6 exemplifies typical transient dynamics of the intermittent motor controller in different versions: (1) the full model, which alternates among all four components, i.e., off–off/on–off/off–on/on–on; (2) reduced models that alternate only between two components, namely off–off/on–off, off–off/off–on, and off–off/on–on.

Fig. 6(a) shows that the upright state of the full intermittent model can reach dynamic equilibrium in the whole range of values of K_h. The two traces at the bottom of Fig. 6(a) represent the patterns of activation/inactivation of the active torques at the ankle and hip, showing that all the four combinations occur with variable time-windows. In particular, the off–off model component operates in a substantial amount of time and, in spite of such absence of active torques, the total CoM angle (θ_{CoM}) gets closer to the upright state. It can be confirmed that those behaviors are dominated by the stable dynamic mode with the associated stable manifold $E^{\mathrm{s,in}}_{\mathrm{off-off}}\oplus E^{\mathrm{s,anti}}_{\mathrm{off-off}}$ of the off–off model. In general, the finite state machine that corresponds to the intermittent controller goes through about 2–3 transitions per second.

3.1. Evidence for intermittent ankle, hip, and mixed strategies

Fig. 6(a)-right-column represents the dynamics for large K_h ($K_h/mgh=1.0$). In this case, changes in the hip angle (θ_h) are small, and the total CoM sway(θ_{CoM}), which is quite close to the ankle angle (θ_a), approaches the upright state almost monotonically. We can also observe that most activation/ inactivation transitions affect the ankle joint, leaving the hip joint inactivated most of the time. We refer to such intermittent control mode as *the intermittent ankle strategy*. In comparison, the dynamics of the intermittent control model shown in the left and middle columns of Fig. 6(a) for small and medium K_h values may be referred to as *intermittent hip strategy* and *intermittent mixed strategy*, respectively. In other words, for the ankle strategy to be feasible the hip stiffness must be sufficiently high.

The performance of reduced controllers, which can only alternate between two of the four model components, helps understanding the different intermittent stabilization strategies (see Fig. 6(c)). For example, the bottom row of the figure (off–off/on–on reduced controller) shows that activating both joints at the same time achieves stability of the target posture regardless of the value of K_h. Moreover, the left column of Fig. 6(c) shows that, for small values of K_h, the critical role for stabilization is played by the hip joint because the control fails if no active torque is provided to that joint. We refer to this as "intermittent hip strategy".

In contrast, for medium values of the hip stiffness (see Fig. 6(c)), the activation of the hip joint is insufficient for stability unless is supported by the simultaneous activation of the ankle. We refer to this as "intermittent mixed strategy".

Fig. 6(a) contains important information on the oscillatory and non-oscillatory modes exhibited by the intermittent motor controller. By definition, the full intermittent controller, which alternates among the off–off, on–off, off–on, on–on components can exhibit the different oscillatory patterns (in-phase and anti-phase) that characterize these components. The lower and upper links move together in the periods of time during which the dynamics of the pendulum is dominated by the in-phase mode, whereas they move in opposite directions in other periods of time during which the dynamics is dominated by the anti-phase mode. The second and third traces in Fig. 6(a) show the in-phase and anti-phase decompositions of the overall sway patterns depicted in the first row of the figure. They show that fractions of the in-phase and anti-phase components depend on the value of K_h: the smaller the value of K_h is, the larger is the fraction of the anti-phase component, implying that the hip joint movement becomes dominant as K_h decreases. In contrast, the larger the value of K_h is, the larger is the fraction of the in-phase component, implying that the ankle joint movement becomes dominant as K_h increases. See Appendix E for the decomposition procedure.

3.2. The patterns of activation/inactivation of the active torques are strategy-dependent

As shown in Fig. 6(a), patterns of activation/inactivation of the active torques correspond to the switchings among the four control model components. Such patterns are K_h-dependent and characterize the three intermittent strategies. Let us look at the second half of the activation patterns for each column of Fig. 6(a), i.e., the quasi-"steady state" patterns: for each K_h value, we can identify the presence of repeated base cycles. In the figure, the beginning of each cycle (chosen as the time instant at which both active torques are inactivated) is marked by a dashed line. Fig. 6(b) shows a magnifications of the patterns including several base cycles.

In particular, for small values of K_h, the pattern in Fig. 6(b)-left-column shows that the base cycle, after the initial off–off phase, continues by switching to the on–off model component at the instant indicated by 'a', then to the off–on model at time 'b', again to the on–off model at time 'c', and finally back to the off–off model at time 'd'. Since two time windows during which the on–off model is active are quite short, we may conclude this dynamic regime is basically an "intermittent hip strategy". For medium

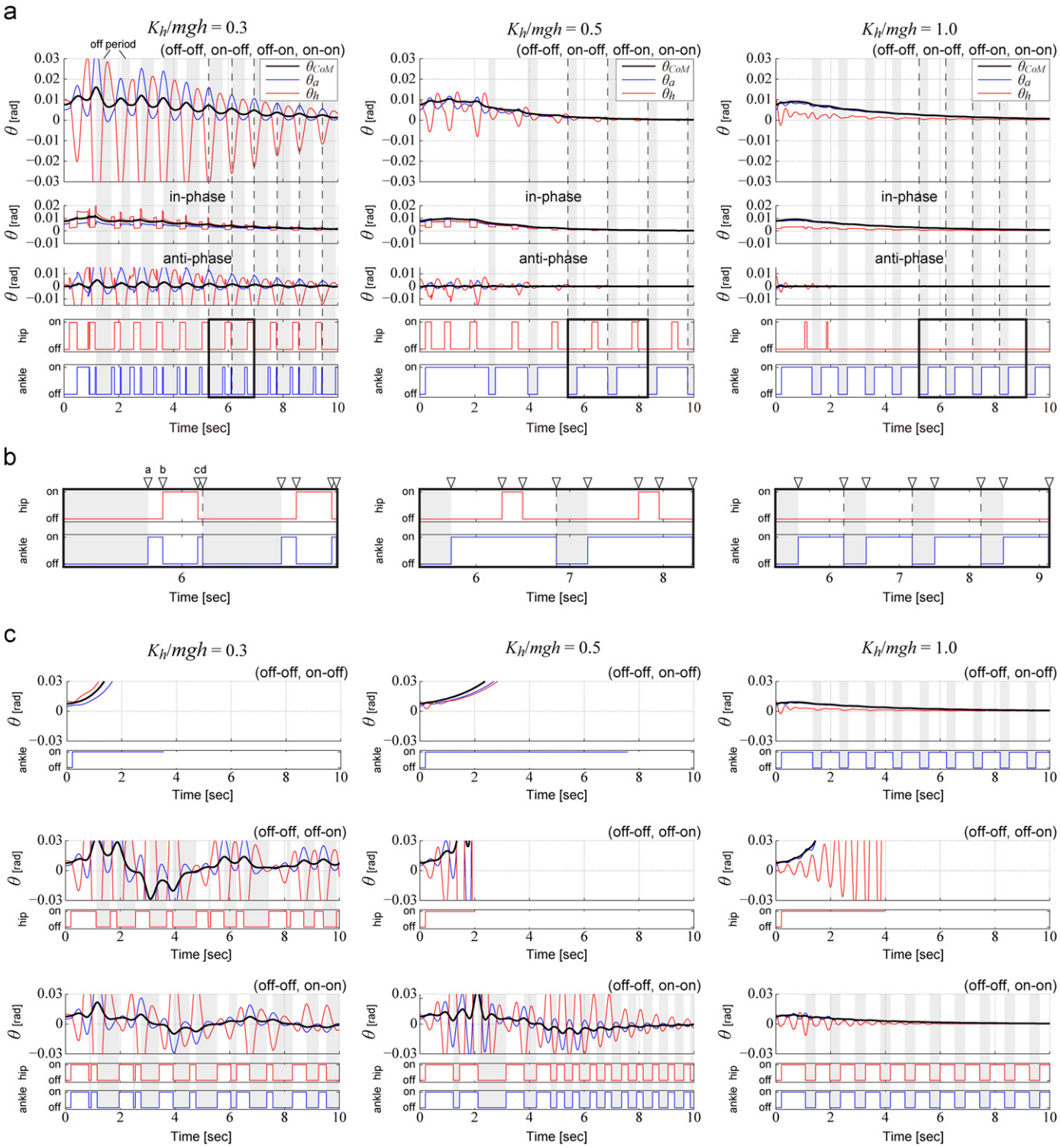

Fig. 6. Transient dynamics of the intermittent control model with different values of the passive hip stiffness K_h ($K_a/mgh = 0.8$, $B_a = 4$ N m s/rad, $B_h = 10$ N m s/rad, $P_a/mgh = 0.4$, $D_a = 10$ N m s/rad, $P_h/mgh = 0.6$, $D_h = 10$ N m s/rad). Values of K_h/mgh are 0.3 for left column, 0.5 for middle, and 1.0 for right column. In panels with θ for vertical axes, black, blue, and red curves represent θ_{CoM}, θ_a, and θ_h, respectively. Traces with square waves represent activations (on) and inactivations (off) of the active torques at the ankle and hip joints. Vertical gray bands in each panel represent the time windows where the system's dynamics are governed by the off–off model with no active torques. (a) Dynamics of the complete intermittent controller (with all possible commutations among off–off/on–off/off–on/on–on model components). Traces at the second and third rows were obtained by decomposing the dynamics on the top trace into their in-phase and anti-phase modes. (b) Magnifications of the activation/inactivation traces shown in (a) in the time interval marked by the bold black rectangle. (c) Dynamics of the reduced intermittent controller, with restricted commutations: off–off/on–off (top row); off–off/off–on (middle row); off–off/on–on (bottom row). For each simulation, the initial state ($t = 0$) was set as follows: $\theta_a = 0.005$ rad, $\theta_h = 0.01$ rad, $\omega_a = 0$ rad/s, and $\omega_h = 0$ rad/s; also the state memory was null: $\theta_a([-\Delta,0]) = \theta_h([-\Delta,0]) = \omega_a([-\Delta,0]) = \omega_h([-\Delta,0]) = 0$, with $\Delta = 0.2$ s.

values of K_h (Fig. 6(b)-middle-column) the base cycle is characterized by a different switching pattern among model components: off–off → on–off → on–on → on–off, and then back to the off–off model. Thus, the cycle can be characterized as an "intermittent mixed strategy". For large values of K_h Fig. 6(b)-right-column shows that emergent strategy is clearly an "intermittent ankle strategy", with permanently inactivated active hip torque.

In summary, by changing the hip stiffness in a rather large range of physiologically plausible values, we obtain different behaviors characterized by different strategies. However, the CoM (black trace in Fig. 6(a)) appears to converge to equilibrium after a transient determined by the initial conditions of the simulations. This is apparent if we observe the traces globally or "stroboscopically", i.e., at the beginning of each cycle. How can the intermittent model generate such convergent dynamics? Apart from the empirical observation of the convergent behavior, a more formal analysis is presented in Section 5, also taking into account the dynamic analysis of the four model components provided by Section 2.

3.3. Robust stability against changes in the active gain parameters

Let us re-examine Fig. 5(b) for assessing the robust stability of the intermittent control model against changes in the active gain parameters. As previously mentioned, for every fixed K_h value, the parameter set (P_a,D_a,P_h,D_h) specifies the intermittent control model. Thus, any point in the (P_a/mgh, D_a,D_h)-space for each given value of P_h/mgh specifies the corresponding intermittent control model.

Fig. 5(b) displays a number of red points in the (P_a/mgh,D_a, D_h)-space for each (K_h/mgh,P_h/mgh). Each red point indicates that the upright state of the intermittent control model defined by that parameter point is stable. Although the sets of parameter point examined are discrete within the range of our investigation, we can confirm that the stability region of the intermittent control model is much wider than that of the continuous on–on model for any K_h value. Thus, we conclude that stability of the intermittent control model is robust against changes in the active gain parameters.

4. Postural sway and energetics in the intermittent control model

4.1. Stochastic postural sway with noise

Let us now consider how postural sway patterns of the intermittent control model are modified by adding white noises to the joint torques. The following equation of motion must be considered:

$$\mathbf{M}\ddot{\boldsymbol{\theta}}+\mathbf{G}\boldsymbol{\theta}=\mathbf{Q}+\sigma\boldsymbol{\xi} \tag{25}$$

where $\sigma\boldsymbol{\xi}=\sigma(\xi_a,\xi_h)^{\mathrm{T}}$ represents the torque noise vector with noise intensity σ. We assume that the ankle torque noise ξ_a and the hip torque noise ξ_h are the standard Gaussian white noise, independent sources. We consider a physiologically plausible level of noise intensity ($\sigma=0.2$ N m), which is compatible with the experimentally estimated intensity of the torque noise due to hemodynamics during human upright standing (Conforto et al., 2001). This small intensity, which was also used in intermittent control models of the single inverted pendulum model (Bottaro et al., 2008; Asai et al., 2009), is about 10 times smaller than the noise level required by continuous control models (Maurer and Peterka, 2005; Van Der Kooij and De Vlugt, 2007; Vette et al., 2010) in order to produce physiological amplitudes of sway movements.

Fig. 7 shows typical postural sway patterns generated by the intermittent control model with the noise input for $K_h/mgh=0.3$, 0.5, and 1.0. The intermittent control model with those three values of the passive hip stiffness behaves stochastically, but in qualitatively different manners, reflecting the corresponding intermittent strategies, namely, the hip, mixed, and ankle strategies, as shown in Section 3 for the noise-less dynamics. For the small K_h, the stochastic postural sway exhibits large and high frequency anti-phase oscillations superposed on the slow in-phase trend, according to the intermittent hip strategy. For the medium K_h, the sway exhibits both monotonic in-phase trend and anti-phase oscillations comparably, reflecting the mixed strategy. For the large K_h, the sway mostly exhibits slow in-phase dynamics, according to the ankle strategy.

Fig. 8 compares two descriptors of simulated and experimental sway patterns, namely power spectral density (PSD) functions and sway histograms of the CoP (Center of Pressure). The experimental data were taken from the public database at www.physiome.jp and correspond to sway movements from two young healthy subjects A and B during human quiet standing samples that span 70 s (Nomura et al., 2009). The simulation data correspond to 10 samples of 300 s, similar to the patterns of Fig. 7. The CoP, in this case, was obtained using a relationship between the ankle torque and CoP (Morasso et al., 1999).

Panel (a) refers to simulated data and panel (b) to experimental data. The PSD for small K_h ($K_h/mgh=0.3$) with the intermittent hip strategy exhibits two dominant resonant peaks at about 1 Hz and 2 Hz, corresponding to the characteristic oscillation frequencies of the anti-phase modes (see Appendix C). The height of each peak in the PSDs becomes less prominent as K_h increases because the intermittent ankle strategy becomes dominant. The resonant peaks almost disappear for large K_h, leading to the PSD with double power law shape similar to PSD obtained in the intermittent control model with a single inverted pendulum (Asai et al., 2009). Thus, appearance of the most prominent resonant peak around 1 Hz could be a hallmark indicating the intermittent hip strategy and/or the mixed strategy as the underlying control strategy. The histogram of the CoP sway with the intermittent hip strategy exhibits a unimodal distribution for the small K_h. However, this distribution tends to become bimodal as K_h increases, reflecting slow in-phase oscillations that are typical for the intermittent ankle strategy, in agreement also with what reported by Bottaro et al. (2008).

The two subjects depicted in panel (b) of Fig. 8 were chosen from the database because they exemplify the qualitative coordination patterns emerging from the simulation study. In particular, subject A has a peak in the PSD at about 2 Hz, which is consistent with a small-medium value of the hip stiffness, but has clearly a unimodal CoP histogram that suggests a low level of hip stiffness. In conclusion, in this subject the hip strategy has definitely a role and he probably operates on the border between a mixed and purely hip intermittent strategies. In contrast, subject B exhibits the typical patterns of a pure ankle strategy, which is considered as the standard of young healthy subjects. However, these are just two examples. Thorough comparisons between experimental and simulated postural sway are beyond the scope of the present work.

4.2. Energy consumption for maintaining the upright posture

We evaluated energy consumption necessary for maintaining the upright posture of the double pendulum by the continuous and the intermittent strategies. The energy consumptions (power) by the passive and active torques were calculated during stochastic postural sway with additive noise, simply as follows:

$$\frac{1}{T}\int_0^T \left|\tau_h^{\mathrm{passive}}(t)\omega_h(t)\right|+\left|\tau_a^{\mathrm{passive}}(t)\omega_a(t)\right| dt$$

$$\frac{1}{T}\int_0^T \left|\tau_h^{\mathrm{active}}(t)\omega_h(t)\right|+\left|\tau_a^{\mathrm{active}}(t)\omega_a(t)\right| dt$$

where the integration time span T was set to 300 s.

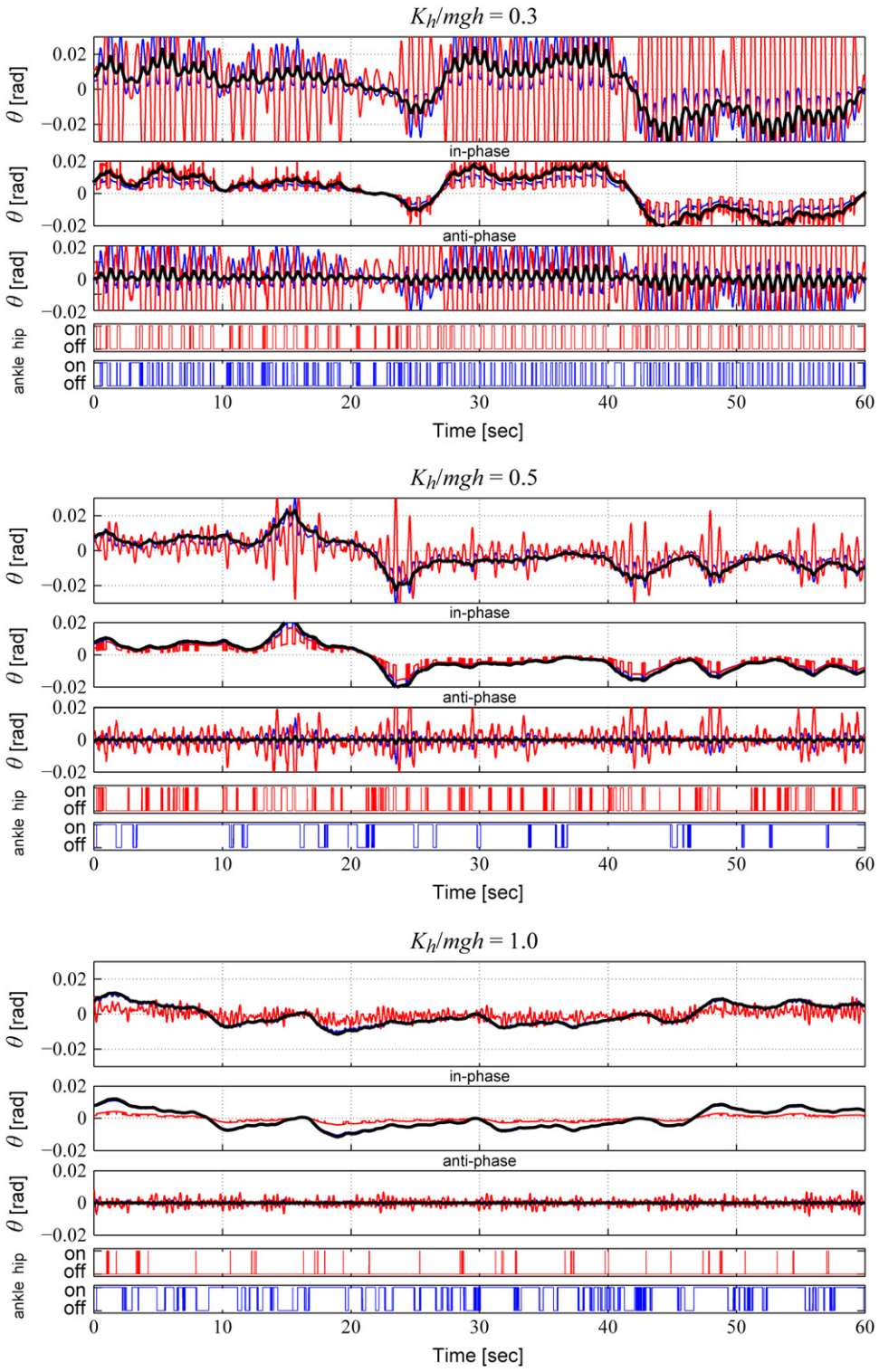

Fig. 7. Postural sways in the intermittent control model with additive white noise for small, medium, and large values of K_h ($K_a/mgh = 0.8$, $B_a = 4$ N m s/rad, $B_h = 10$ N m s/rad, $P_a/mgh = 0.4$, $D_a = 10$ N m s/rad, $P_h/mgh = 0.6$, $D_h = 10$ N m s/rad, $\Delta = 0.2$ s, $\sigma = 0.2$ N m). Blue, red, and thick black curves represent the angles of the ankle joint θ_a, the hip joint θ_h, and the total CoM θ_{CoM}. For each value of K_h, the five rows represent the following variable: (1) the angular oscillations (θ_a,θ_h,θ_{CoM}); (2) the decomposed in-phase waveforms; (3) the decomposed anti-phase waveforms; (4) the activations/inactivation signals of the active hip torque; (5) the activations/inactivation signals of the active ankle torque. The sway patterns for the three values of K_h/mgh reflect dynamic characteristics of the three intermittent strategies: hip, mixed, and ankle, respectively.

Energy consumption during stochastic postural sway in the continuous control model with $P_a/mgh = 0.4$, $D_a = 70$ N m s/rad, $P_h/mgh = 0.2$, and $D_h = 3$ N m s/rad (located at the center of the narrow stability region shown in Fig. 5(b)) for $K_h/mgh = 1.0$ was about 1580 mW in total, in which the passive power at the ankle and hip were, respectively, about 115 and 840 mW, and the active power at the ankle and hip were, respectively, about 65 and 560 mW. While in the intermittent control model with the ankle strategy for $K_h/mgh = 1.0$, it was about 110 mW in total, in which the passive power at the ankle and hip were, respectively, about

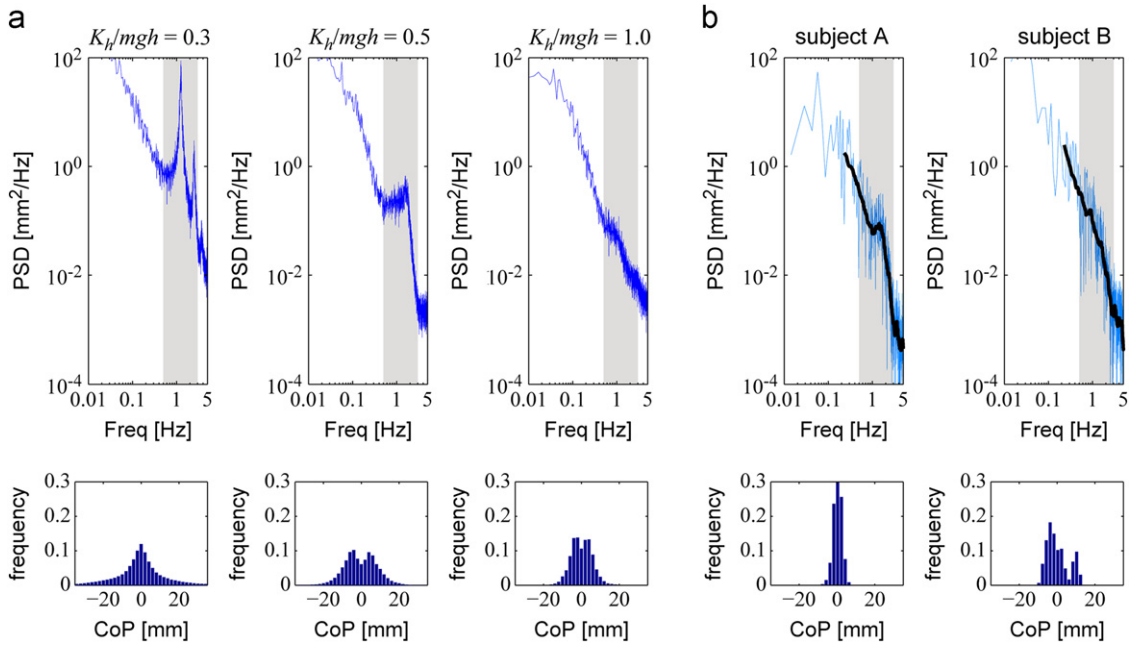

Fig. 8. Power spectral density (PSD) functions and sway histograms of the center of pressure (CoP) in the intermittent control model and human sway. In the simulated data, the CoP was derived from the ankle joint torque; the PSDs were then obtained by averaging 10 samples of 300 s. In the human case, the CoP is part of the measurements. (a) Left, middle, and right columns are PSD (upper) and histogram (lower) for $K_h/mgh = 0.3$, 0.5, and 1.0, respectively. (b) Left and right columns are PSD and histogram for the CoP sways from human subjects A and B, respectively, during quiet standing.

30 and 65 mW, and the active power at the ankle and hip were, respectively, about 12 and 3 mW. This means that energy efficiency of the intermittent control model was about 10 times better than that of the continuous control model. Note that, in these energy estimations, we assumed different noise intensity σ for simulating postural sway of the identical variance in the two different models; $\sigma = 0.33$ N m/rad for the continuous control model and $\sigma = 0.2$ N m/rad for the intermittent control model.

Such comparisons could not be performed for smaller passive hip stiffness ($K_h/mgh = 0.3$ and 0.5), because the continuous control model could not stabilize the upright posture for these small K_h values. Nevertheless, the total powers during the mixed ($K_h/mgh = 0.5$) and the hip ($K_h/mgh = 0.3$) strategies were, respectively, about 570 and 5700 mW. That is, the mixed strategy for the medium passive hip stiffness is still two times more energy efficient than the continuous control model for the large hip stiffness.

5. Understanding dynamics of the intermittent control model

The dynamics of intermittent control models, exemplified by the graphs of Fig. 6(a) in the absence of noise, are re-analyzed here in order to better understand how the intermittent strategies can stabilize the upright state of the double pendulum. We described state-dependent switching rules among the model components, by which the active torques acting on the ankle and hip joints are selectively activated when the intermittent controller finds out that the delayed estimate of the state vector $x(t-\Delta)$ overcomes a safety distance from the stable manifold of the off–off model. We expected, as the simulations seem to indicate, that the active torques turned on by that event were able to pull the system's state back to the safe neighborhood of the stable manifold of the off–off model, after some period of time. How is this achieved in the dynamics shown in Fig. 6(a)?

It is certainly true that when the system's state is in the neighborhood of the stable manifold of the off–off model it tends to approach the target upright position, but only transiently and thus we must face another question: How does this transient behavior of the off–off model component combine with the unstable dynamics of the DDE model components for stabilizing the overall dynamics? To answer these questions, we consider the approximated manifolds of the approximated ODE (a-ODE) model components to decompose the dynamics of the corresponding DDE model components. Figs. 9–11 reuse the dynamics shown in the left ($K_h/mgh = 0.3$), middle ($K_h/mgh = 0.5$), and right ($K_h/mgh = 1.0$) panels of Fig. 6(a), respectively.

5.1. Map representations of the dynamics

For descriptive convenience, we define a map representation of dynamics of the intermittent control model. Suppose one model component governs the dynamics of the system continuously for a time interval $[t_s,t_f]$ during which the system's state evolves from the initial state p_s to the final state p_f. This change can be described as a mapping from p_s to p_f. Note that p_s and p_f represent, respectively, the state functions $x([t_s-\Delta,t_s])$ and $x([t_f-\Delta,t_f])$ if the governing model component is one of the DDE defined by Eq. (15). They represent the state points $x(t_s)$ at $t = t_s$ and $x(t_f)$ at $t = t_f$ in the four-dimensional state space E if the governing model component is the off–off model component.

We denote the flow of the system as F_i with i=off–off, on–off, off–on, and on–on. For example, the flow $F_{\text{on-on}}$ represents the map when dynamics of the system is governed by the on–on model component. The map F_i relates p_s and p_f as follows:

$$p_f = F_i(p_s) \tag{26}$$

5.2. Intermittent hip strategy for small K_h

Fig. 9(a) redisplays a part of dynamics of the intermittent control model shown in Fig. 6(a)-left for small K_h. The extracted

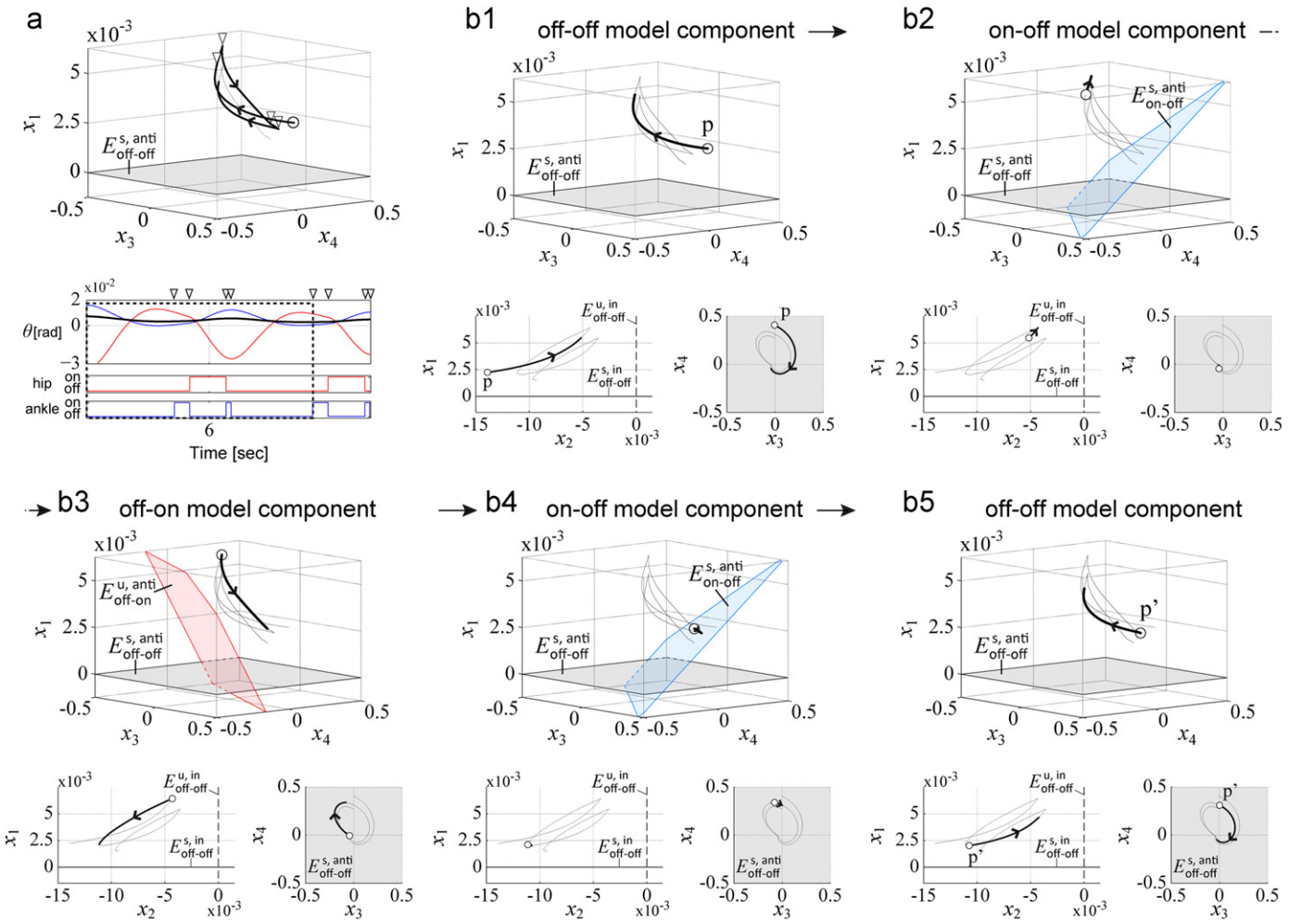

Fig. 9. Dynamics with the intermittent hip strategy ($K_h/mgh = 0.3$). Dynamics shown in Fig. 6(a)-left are plotted again. (a) Trajectory projected in the state space E (upper) and the corresponding joint angles and activation/inactivation of the active torques (lower). The ○ maker in the E represents the state (head) of the system at the beginning of the waveforms in the lower panel surrounded by dotted square. Four ▽ makers indicate switching of the model components. (b) Dynamics shown in (a) is dissected into five fragments, governed by specific model components: off–off (b)-1; on–off (b)-2; off–on (b)-3; on–off (b)-4; off–off again (b)-5. The ○ marker in each panel represents the state (head) of the system immediately after the commutation of the model component. Planes colored in blue or red in each panel represent the manifold associated with the dominant mode.

portion is identified by the bold rectangle in Fig. 6(a)-left and is expanded for convenience in Fig. 6(b)-left. In Fig. 9(a), the marker ○ in E represents the state point $p = x(t_s)$ at the beginning of the extracted portion, which is just after the model component is switched to the off–off model; the cycle continues with a sequence of commutations of model components, whose timing is indicated by ▽ markers as follows: off–off → on–off → off–on → on–off and then switched back to the off–off model component.

The basic cycle of Fig. 9(a) is broken down into its fragments (Fig. 9(b)-1 to (b)-5), each of which is governed by one of the model components (off–off, on–off, off–on, and on–off, respectively). The ○ marker in Fig. 9(b)-2 to (b)-4 represents the head of the state function at the onset of each period. The time evolution of the state starting from the point p in (b)-1 at the onset of the base cycle to the point p' in (b)-5 at the onset of the next base cycle can be described as follows:

$$p' = F_{\mathrm{on-off}} \circ F_{\mathrm{off-on}} \circ F_{\mathrm{on-off}} \circ F_{\mathrm{off-off}}(p) \equiv F_{\mathrm{hip}}(p) \tag{27}$$

As one can observe in Fig. 9(b)-1, the trajectory governed by the off–off model component from p to $F_{\mathrm{off-off}}(p)$ exhibits a hyperbolic curve segment in the x_1–x_2 plane, where the x_2-coordinate approaches the zero along $E^{\mathrm{s,in}}_{\mathrm{off-off}}$ for the early period, and then the x_1-coordinate increases gradually away from the zero along $E^{\mathrm{u,in}}_{\mathrm{off-off}}$. In the x_3–x_4 plane, it forms a spiral curve segment approaching the origin as determined by $E^{\mathrm{s,anti}}_{\mathrm{off-off}}$.

Since $F_{\mathrm{off-off}}(p)$ goes outside the safe neighborhood of the stable manifold of the off–off model, the system's controller switches to the on–off model component in order to evolve from $F_{\mathrm{off-off}}(p)$ to $F_{\mathrm{on-off}} \circ F_{\mathrm{off-off}}(p)$, because this commutation allows the tail of the state function to stay inside the safe neighborhood of the stable manifold of the on–off model. However, in Fig. 9(b)-2, the tail of the state departs from the neighborhood of the stable manifold of the on–off model component after a short period, and the system is then governed by the off–on model component to evolve from $F_{\mathrm{on-off}} \circ F_{\mathrm{off-off}}(p)$ to $F_{\mathrm{off-on}} \circ F_{\mathrm{on-off}} \circ F_{\mathrm{off-off}}(p)$. In Fig. 9(b)-3, the off–on model component succeeds to pull back the state of the system closer again to the stable manifold of the off–off model, where the unstable anti-phase oscillation generated only by the active hip torque plays a dominant role. Before returning to the off–off model component, the intermittent controller activates for a short time the on–off model component, since $F_{\mathrm{off-on}} \circ F_{\mathrm{on-off}} \circ F_{\mathrm{off-off}}(p)$ enters into the neighborhood of the stable manifold of the on–off model. Eventually, the system's state reaches p' back into the neighborhood of the stable manifold of the off–off model, closing the cycle.

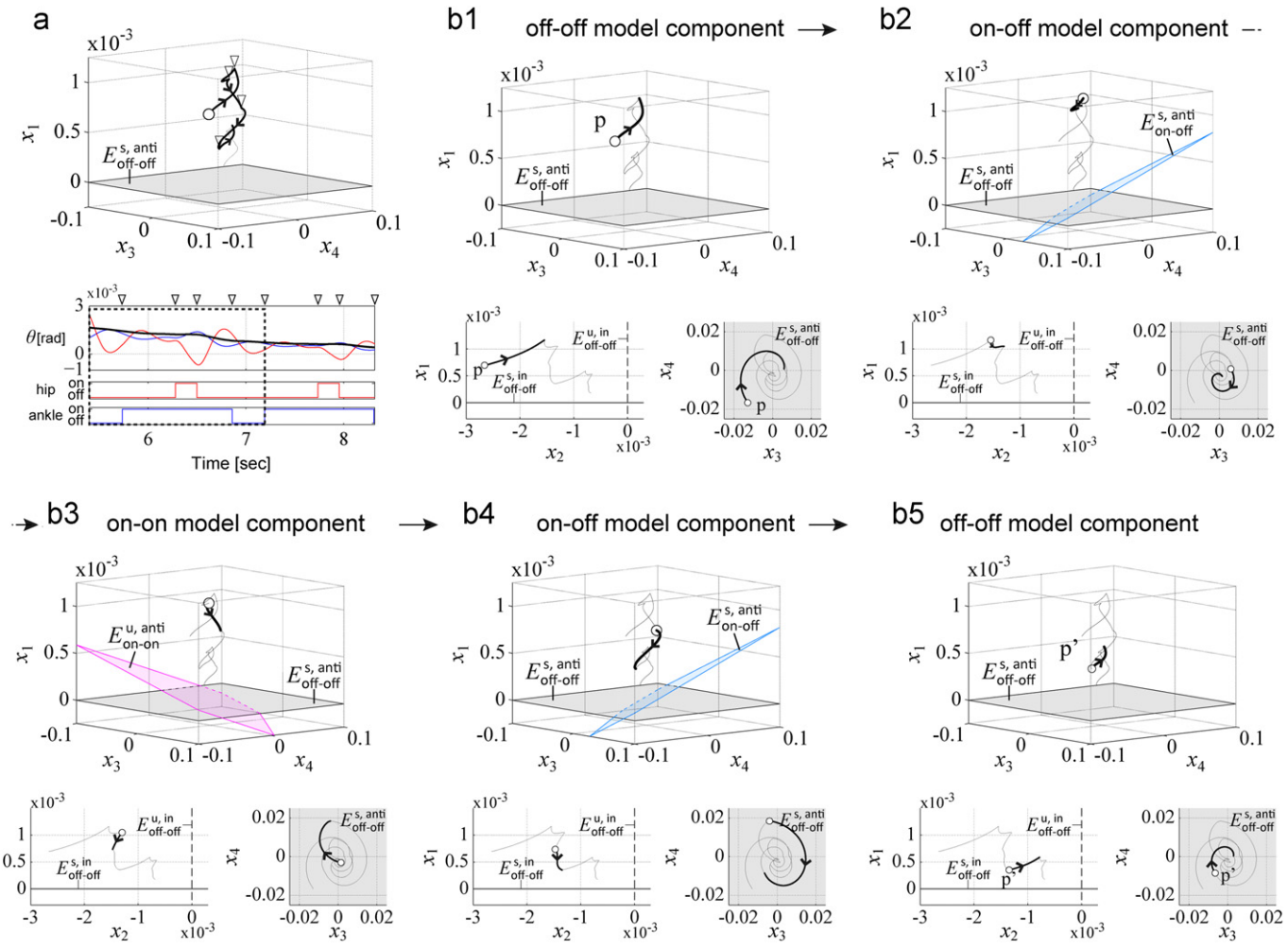

Fig. 10. Dynamics with the intermittent mixed strategy ($K_h/mgh = 0.5$). Dynamics shown in Fig. 6(a)-middle are plotted again. See legend of Fig. 9.

The relevant point is that if we compare the initial location of the system's trajectory (p in panel (b)-1) with the final location (p' in (b)-5) we can verify that $|p| > |p'|$. This implies that the map F_{hip} is convergent, when it is operated iteratively for successive base cycles. Therefore, the fixed point of F_{hip} is the origin, and the stability of the origin is dominantly determined by the rate of transient approach from p to $F_{\mathrm{off-off}}(p)$ and the rate of divergence from $F_{\mathrm{on-off}} \circ F_{\mathrm{off-off}}(p)$ to $F_{\mathrm{off-on}} \circ F_{\mathrm{on-off}} \circ F_{\mathrm{off-off}}(p)$. Fig. 9(b) shows that $F_{\mathrm{off-off}}(p)$ is closer to the origin than p, and $F_{\mathrm{off-on}} \circ F_{\mathrm{on-off}} \circ F_{\mathrm{off-off}}(p)$ is slightly more distant from the origin than $F_{\mathrm{on-off}} \circ F_{\mathrm{off-off}}(p)$. The origin is stable because the former transient approaching rate is greater than the latter diverging rate.

Analyzing the manifold-wise representation of each fragment of the dynamics (see Appendix E), we obtain the following transitions and the manifolds dominating the dynamics for the intermittent hip strategy:

$$E^{\mathrm{u,in}}_{\mathrm{off-off}} \oplus \overline{E^{\mathrm{s,in}}_{\mathrm{off-off}}} \oplus \overline{E^{\mathrm{s,anti}}_{\mathrm{off-off}}} \to \overline{E^{\mathrm{u,in}}_{\mathrm{off-off}}} \oplus E^{\mathrm{s,in}}_{\mathrm{off-off}} \oplus E^{\mathrm{s,anti}}_{\mathrm{off-off}}$$
$$\to E^{\mathrm{u,in}}_{\mathrm{on-off}} \oplus \overline{E^{\mathrm{s,in}}_{\mathrm{on-off}}} \oplus \overline{E^{\mathrm{s,anti}}_{\mathrm{on-off}}} \to E^{\mathrm{u,in}}_{\mathrm{off-on}} \oplus E^{\mathrm{s,in}}_{\mathrm{off-on}} \oplus \overline{E^{\mathrm{u,anti}}_{\mathrm{off-on}}}$$
$$\to E^{\mathrm{u,in}}_{\mathrm{on-off}} \oplus \overline{E^{\mathrm{s,in}}_{\mathrm{on-off}}} \oplus \overline{E^{\mathrm{s,anti}}_{\mathrm{on-off}}}$$

Here any model component that is dominantly used for a period of time over 15% of one base cycle is emphasized by surrounding the corresponding set of manifolds with a box. The on–off model component governs the dynamics only for short periods of time, and it does not contribute much to pulling the state back to the stable manifold of the off–off model. Thus, we conclude that the off–off and the off–on model components are dominantly utilized in the intermittent hip strategy, in which the unstable manifold $E^{\mathrm{u,anti}}_{\mathrm{off-on}}$ associated with the oscillatory anti-phase mode $M^{\mathrm{u,anti}}_{\mathrm{off-on}}$-osc of the off–on model and the stable manifold associated with the monotonic in-phase mode $M^{\mathrm{s,in}}_{\mathrm{off-off}}$-mon and the oscillatory anti-phase mode $M^{\mathrm{s,anti}}_{\mathrm{off-off}}$-osc of the off–off model stabilize the upright state.

5.3. Intermittent mixed strategy for medium K_h

Similarly, Fig. 10 redisplays a part of dynamics of the intermittent control model shown in Fig. 6(a)-middle for medium K_h. In this case, the model components are switched as follows: off–off → on–off → on–on → on–off, and then back to the off–off model. As in the hip strategy case, the time evolution from p in (b)-1 at the beginning to p' in (b)-5 at the onset of the next base cycle can be described as follows:

$$p' = F_{\mathrm{on-off}} \circ F_{\mathrm{on-on}} \circ F_{\mathrm{on-off}} \circ F_{\mathrm{off-off}}(p) \equiv F_{\mathrm{mixed}}(p) \tag{28}$$

The trajectory from p to $F_{\mathrm{off-off}}(p)$ shown in Fig. 10(b)-1 is governed by the off–off model as in Fig. 9(b)-1. Since $F_{\mathrm{off-off}}(p)$ becomes away from the stable manifold of the off–off model but closed to the stable manifold of the on–off model, the system is governed by the on–off model from $F_{\mathrm{off-off}}(p)$ to $F_{\mathrm{on-off}} \circ F_{\mathrm{off-off}}(p)$ as in Fig. 10(b)-2. Unlike in the hip strategy case, the stable

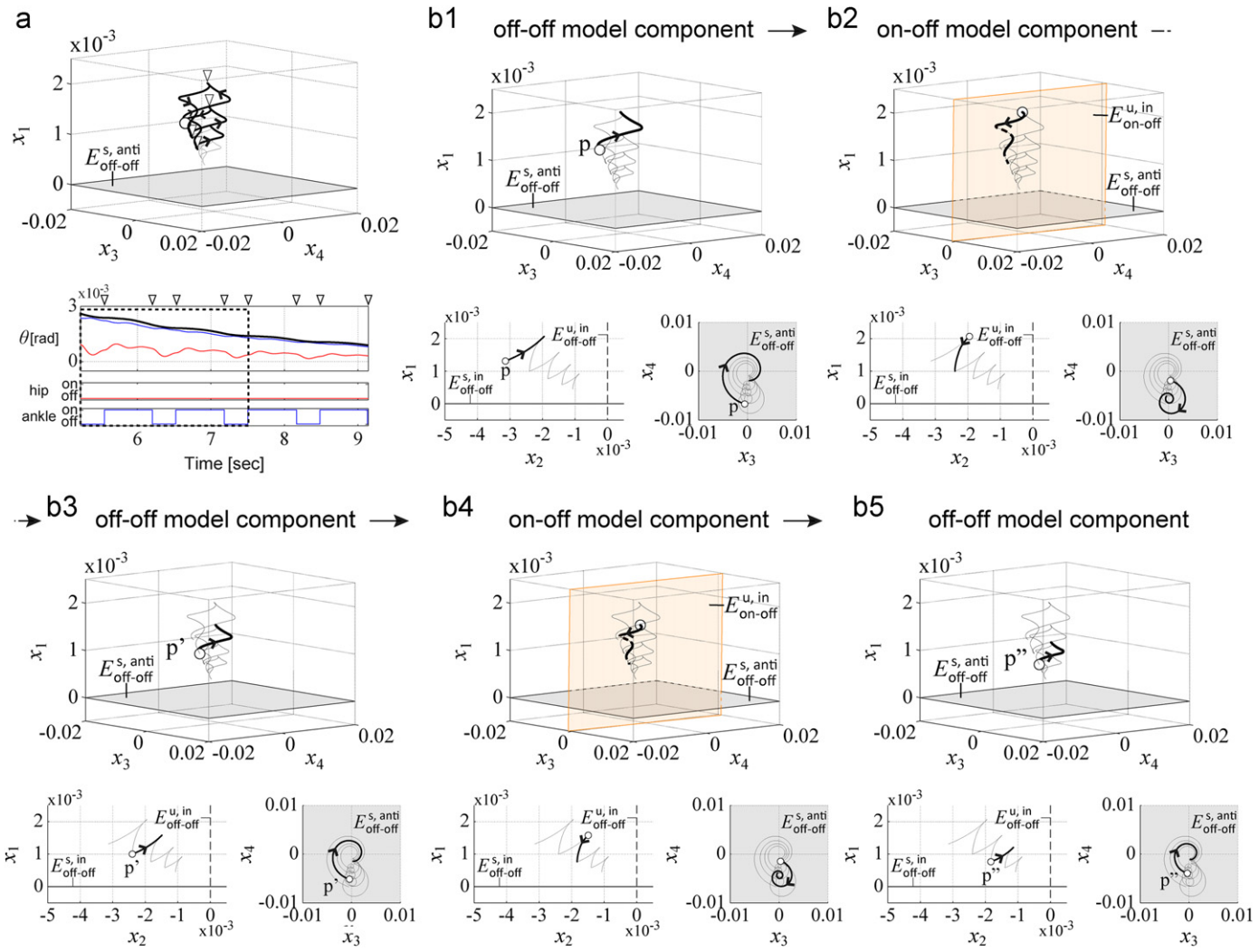

Fig. 11. Dynamics with the intermittent ankle strategy ($K_h/mgh = 1.0$). Dynamics shown in Fig. 6(a)-right are plotted again. See legend of Fig. 9.

manifold $E^{s,anti}_{on-off}$ of the on–off model partly contributes to pulling the state closer to the stable manifold of the off–off model. Then, in Fig. 10(b)-3, the system is governed by the on–on model from $F_{on-off} \circ F_{off-off}(p)$ to $F_{on-on} \circ F_{on-off} \circ F_{off-off}(p)$, where dynamics of the on–on model dominated by $E^{u,anti}_{on-on}$ pulls the state of the system further close to the stable manifold of the off–off model. The state of the system is then governed again by the on–off model. Dynamics of the on–off model dominated by $E^{s,anti}_{on-off}$ gets the system's state reached at p' closed to the stable manifold of the off–off model. Comparison of the location of p in (b)-1 with that of p' in (b)-5 shows $|p| > |p'|$, implying that the map F_{mixed} is also convergent when it is operated iteratively.

The manifold-wise representation gives the following transitions and the manifolds dominating the dynamics for the intermittent mixed strategy:

$$E^{u,in}_{off-off} \oplus \overline{E^{s,in}_{off-off}} \oplus \overline{E^{s,anti}_{off-off}} \to \overline{E^{u,in}_{off-off}} \oplus E^{s,in}_{off-off} \oplus E^{s,anti}_{off-off}$$
$$\to E^{u,in}_{on-off} \oplus \overline{E^{s,in}_{on-off}} \oplus \overline{E^{s,anti}_{on-off}} \to E^{u,in}_{on-on} \oplus \overline{E^{u,anti}_{on-on}}$$
$$\to E^{u,in}_{on-off} \oplus \overline{E^{s,in}_{on-off}} \oplus \overline{E^{s,anti}_{on-off}}$$

In this case, each of the three model components operates for a comparable period of time, exceeding 15% of one base cycle. Thus we may conclude that in the intermittent mixed strategy the off–off, on–off, and on–on model components are utilized in an equally dominant way.

5.4. Intermittent ankle strategy for large K_h

As in the two cases above, Fig. 11(a) redisplays a part of the dynamics of the intermittent control model shown in Fig. 6(a)-right for large K_h. In this case, the model components are switched simply between the off–off and the on–off models. In Fig. 11(b), two and a half base cycles are extracted from the data shown in Fig. 6(a)-right. The corresponding dynamics from p in (b)-1 to p' in (b)-3 at the onset of the next base cycle, and then to p'' in (b)-5 at the second onset of the subsequent base cycle, can be described as follows:

$$p' = F_{on-off} \circ F_{off-off}(p_s) \equiv F_{ankle}(p) \quad (29)$$

$$p'' = F_{ankle}(p') \quad (30)$$

The dynamics from p to $F_{off-off}(p)$ in Fig. 11(b)-1 is the same as the two cases above. When the state reaches $F_{off-off}(p)$, the control is switched to the on–off model until the state reaches $F_{on-off} \circ F_{off-off}(p)$. In Fig. 11(b)-2, the unstable manifold $E^{u,in}_{on-off}$ of the on–off model largely contributes to pulling the state closer to the stable manifold of the off–off model, leading to the state point $p' = F_{on-off} \circ F_{off-off}(p)$ back in the safe neighborhood of the

stable manifold of the off–off model. This means that the unstable oscillatory in-phase mode generated only by the active ankle torque plays a dominant role in the intermittent ankle strategy. The second base cycle starts from $p' = F_{\mathrm{on-off}} \circ F_{\mathrm{off-off}}(p)$ and then repeats qualitatively the same dynamic as shown in Fig. 11(b)-3 and (b)-4, then reaching the state point p'' at the onset of the third cycle (the early half) shown in Fig. 11(b)-5. We can show that $|p| > |p'|$ and $|p'| > |p''|$, implying that the map F_{ankle} is also convergent for iterative operations along successive base cycles.

Using the manifold-wise representation, we obtain the following transition between the dominant manifolds for the intermittent ankle strategy:

$$E^{\mathrm{u,in}}_{\mathrm{off-off}} \oplus \overline{E^{\mathrm{s,in}}_{\mathrm{off-off}}} \oplus \overline{E^{\mathrm{s,anti}}_{\mathrm{off-off}}} \rightarrow \overline{E^{\mathrm{u,in}}_{\mathrm{off-off}}} \oplus E^{\mathrm{s,in}}_{\mathrm{off-off}} \oplus E^{\mathrm{s,anti}}_{\mathrm{off-off}} \rightarrow \overline{E^{\mathrm{u,in}}_{\mathrm{on-off}}} \oplus E^{\mathrm{s,anti}}_{\mathrm{on-off}}$$

In this case, only two model components are utilized, and each of them is utilized for the period of time over 15% of one base cycle. We thus conclude that the stable manifold of the off–off model component and the unstable manifold $E^{\mathrm{u,in}}_{\mathrm{on-off}}$ of the on–off model component are dominantly utilized in the intermittent ankle strategy for stabilizing the upright state.

In summary, the sequences of model components selected by the intermittent controller for stabilizing the upright state are automatically changed as a consequence of the specific value of K_h, while keeping a common switching strategy. Either on–off or on–on model component is always selected regardless of the value of K_h, implying that active ankle torque plays a primary role for stabilizing quiet standing. In particular, the switching between off–off and on–off components is selected for large K_h, in the intermittent ankle strategy. Additional switching is required for small and medium values of K_h. For small K_h, in the intermittent hip strategy, the on–off component mediates the switching between the off–off and the off–on model components, although the role played by the on–off model component is rather scarce. For medium K_h, in the intermittent mixed strategy, on–off and on–on model components are dominant. Note that the roles played by the on–off model component in the hip and mixed strategies and in the ankle strategy are not the same. In the latter case, the unstable oscillatory dynamics pulls the state of the system back to the stable manifold of the off–off model, while in the former case, the stable dynamics contributes to getting the state of the system closer to the upright state.

6. Discussion

In this study, we developed an intermittent control model of a double inverted pendulum that simulates movements of the ankle and hip joints during human upright standing. Parameter values of the model were taken within a physiologically plausible range. In particular, we assumed small passive viscoelasticity at the ankle and hip joints, which makes the upright equilibrium unstable without neural control. Moreover, a large feedback transmission delay makes the stabilization by the active feedback control difficult from a viewpoint of conventional continuous feedback control. We demonstrated the scarce robustness of a continuous controller based on proportional and derivative feedback, by showing that even if the control parameters were optimally tuned, the region of stability in the parameter space was very narrow. In contrast, we showed that the double inverted pendulum model could be stabilized in a robust way by a switching mechanism that generated appropriate sequences of activation/inactivation of active torques at the ankle and hip joints. A clear difference in size of the stability regions in the parameter space between continuous and intermittent control models for stabilizing the double inverted pendulum supports the latter as a better candidate of the strategy employed by the CNS for stabilizing multiple joints in upright standing. Moreover, we showed that the intermittent strategy was much more energetically efficient than the continuous strategy.

The proposed intermittent controller is basically a finite-state machine, which switches from one linear controller to another, thus generating different combinations of active torques at the ankle and hip joints. The simplicity of this mechanism is that there is no complex computation aimed at selecting specific combinations of the active torques for a given passive hip stiffness. The principle of coordination is simply to select a combination of active torques that can pull the state of the system to the stable manifold of the off–off model (not to the upright equilibrium state), without caring about the passive hip stiffness K_h. Remarkably, despite the simplicity of the proposed intermittent control model, three types of strategies or synergies *emerge* spontaneously as a function of the passive hip stiffness K_h: (1) ankle strategy, (2) hip strategy, and (3) mixed strategy. This is a manifestation of the robustness of the intermittent controller because it automatically adapts the strategy as an important parameter, like hip stiffness, undergoes large variations. Moreover, such adaptive switching among possible synergies, which may also be interpreted as a mechanism of redundancy resolution, does not require the specific use of optimal feedback control techniques that in recent years have become the most influential building blocks of the leading theories in the neural control of movement (Todorov, 2004).

The essential mechanism responsible for the robustness and flexible stability of the intermittent control model is the *exploitation* (in the sense of an *affordance*) of the stable manifold of the saddle type unstable upright state exhibited by the double inverted pendulum with no active feedback torques. As in the intermittent control model of the single inverted pendulum (Asai et al., 2009), flexible upright stabilization could be achieved because no active effort was made to get the state of the pendulum close to the upright state, but the stable dynamics of the unstable saddle brought the state of the pendulum to the upright state along the stable manifold without any active effort. This is why the intermittent control is more energetically efficient than the continuous control. The role played by the state-dependent appropriate combinations of the active torques was to move the state of the pendulum across the stable manifold of the saddle. This can be achieved with less effort and more robustness than directly forcing the state of the pendulum asymptotically to the upright state. The proposed intermittent control model is also able to reproduce postural fluctuations comparable to human postural sway by simply adding small additive torque noise (Conforto et al., 2001), suggesting that flexible upright state and compliant dynamics were established by the model rather than driven by the noise.

6.1. Relation with the ballistic, impulsive control

From a general point of view, the proposed intermittent control model is related to the ballistic, impulsive active control considered by Loram and Lakie (2002b) and Loram et al. (2005). First of all, apart from specific underlying mechanisms, they are related simply because both of them consider intermittent and phasic active interventions. Moreover, the upright posture is just a nominal equilibrium that is not directly targeted by the neural controllers in both cases. Instead, both types of controllers exploit a broader set of the system's state: the stable manifold of the non-actively-controlled body pendulum (the off–off model) for the proposed intermittent control model; the instantaneous

quasi-equilibrium when the ankle torque and the gravitational toppling torque balance each other, triggering the activation of the ballistic impulsive control. In other words, events that elicit the interventions are (1) the departure of the system's state from the safe neighborhood of the off–off model, for the proposed intermittent controller, and (2) point of null acceleration (or local maximum of the falling velocity), for the impulsive controller. These two types of events are not necessarily the same but are probably correlated: it is quite likely indeed that the local maximum point of falling velocity occurs when the system's state has just exited the safe neighborhood of the stable manifold of the non-actively-controlled body pendulum, implying that these two events are functionally equivalent from the point of view of the timing mechanism. However, in order to compare the two control models in a more specific way, it is necessary to extend the impulsive controller from a single pendulum to a double pendulum, in order to verify, among other things, to which extent the latter controller can explain the emergence of different types of strategies without additional control mechanisms.

However, it is important to note that the role played by the active interventions triggered by the nearly equivalent events should not be overestimated in the framework of the intermittent control model. This is because the postural stability cannot be established by itself. What is crucial for stabilization is the timing of inactivation of the active intervention, in order to utilize the transient stable behavior near the stable manifold of the non-actively-controlled body pendulum.

6.2. Finite dimensional approximation of the delay differential equations

The intermittent control model proposed in this study utilized the finite dimensional approximations of the delay differential equations (DDE models) as in Eq. (17), i.e., a-on–off, a-off–on, and a-on–on model components, in which only the four dominant modes of each DDE model were taken into account. More specifically, the stable manifold of the on–off DDE model was approximated by the two dimensional manifold of the four dimensional a-on–off model to determine whether the system's state is located near the stable manifold of the on–off model. Moreover, the change rate vector of the physical state of the pendulum at Δ seconds past for the on–off, off–on, and on–on model components defined in Eq. (22) were evaluated approximately using the corresponding a-ODE model components to select a DDE model component used to pull the system's state toward the stable manifold of the off–off model.

One may argue whether each a-ODE model can well approximate dynamics of the corresponding DDE model. We checked carefully that the stability region in the active gain parameter space for each a-ODE model shows fairly good coincidence with that obtained by numerical simulations for the corresponding DDE model. Indeed, the a-ODE models in Eq. (17) can approximate the DDE models much better than the four-dimensional ODE models obtained simply by using Taylor expansions of $\boldsymbol{\theta}(t-\Delta)\sim\boldsymbol{\theta}(t)-\Delta\boldsymbol{\omega}(t)$ and $\boldsymbol{\omega}(t-\Delta)\sim\boldsymbol{\omega}(t)-\Delta d\boldsymbol{\omega}(t)/dt$ for Eq. (15). We have not examined theoretically how much the two-dimensional stable manifold of the a-on–off model can approximate the infinite-dimensional stable manifold of the on–off DDE model. However, by definition of the dominant eigenvalues, all of the infinite number of neglected modes are more stable than those remained for the approximated stable manifold, meaning that the neglected modes vanish faster than the remaining modes. Although the direct sum decompositions of the space E were also based on the a-ODE models, they were just used to understand dynamics of the intermittent control model. Since the obtained interpretations of the dynamics were quite reasonable, we are confident to conclude that the overall dynamics of the intermittent control model can be well captured by the finite dimensional direct sums of the approximated manifolds. Nevertheless, it is worth performing a theoretical analysis of the switching dynamics among the DDE models, such as the study by Simpson et al. (2012) for the single pendulum case.

6.3. Effects of parameter values

It has been shown that the critical value of the passive ankle stiffness required for stabilizing the multi-link model of upright stance is larger than that for the single-link model of the upright stance (Edwards, 2007; Rozendaal and Van Soest, 2008). Similarly, the critical value of the passive hip stiffness required for stabilizing the multi-link model of upright stance is also larger than that required for stabilizing the upper trunk segment alone (Edwards, 2007). The passive ankle stiffness $K_a=0.8mgh$ is 80% of the critical stiffness for the single inverted pendulum. The critical passive hip stiffness for the inverted upper trunk alone is $m_{HAT}gh_{HAT}\sim 0.25mgh$, which is slightly smaller than K_h examined in this study. However, for the double pendulum, the critical stiffness values K_a and K_h are inversely related, where the minimum critical value of K_a is mgh for the infinite hip stiffness and that of K_h is $0.25mgh$ for the infinite ankle stiffness. In between these two extreme cases, the critical hip stiffness is about $0.5mgh$ for $K_a=1.25mgh$, and about $0.8mgh$ for $K_a=1.1mgh$. Thus, the examined range of $K_h/mgh\in[0.3,1.0]$ covers a sufficiently wide range. Stabilizing the upright state becomes difficult for smaller values of K_h than $0.3mgh$ (the smallest value examined) for the fixed K_a at $0.8mgh$ even with the intermittent control model. Thus, $K_h/mgh\sim 0.3$ is about the lowest limit for stabilizing the upright posture by the proposed intermittent control model.

In this study, we fixed the passive hip viscosity at the small value of $B_h=10.0$ N m s/rad. Larger values of B_h make the stabilization of the double pendulum easier, but a variety of dynamics is lost. In particular, we have checked that the intermittent control model exhibits only single-pendulum-like dynamics with the intermittent ankle strategy for $B_h>15$ N m s/rad. For smaller values of B_h, stabilization of the double pendulum becomes difficult even with the use of the intermittent control. The lowest limit of B_h that can stabilize the upright state depends on the passive hip stiffness K_h. It is about 7 and 5 N m s/rad for $K_h/mgh=0.3$ and $K_h/mgh=0.5$, respectively. For $K_h/mgh=1.0$, the upright state can be easily stabilized even for $B_h=0$ N m s/rad.

Regarding the active gain parameters, we have shown simulations of the intermittent control model only with the selected set, which is small and far outside the stability region of each individual continuous control model, to ensure flexibility of the joints. This selection made the control problem difficult. We have examined many other active gain parameter sets, with all the other parameter values fixed, and we are confident to say that stability of the model is quite robust against large variation of them as shown in Fig. 5. In any case, the selected parameter values were the ones that exhibited a physiological variety of coordinated dynamics.

6.4. Coordination and dimensionality

In recent years there has been an increasing number of studies related to coordinated joint movements during quiet standing (Alexandrov et al., 2005; Creath et al., 2005; Hsu et al., 2007; Pinter et al., 2008). In particular, Hsu et al. (2007) performed uncontrolled manifold (UCM) analysis of the postural system, taking into account the study by Scholz and Schoner (1999), and found that the examined six joints during quiet standing were

coordinated such that their combined variance had minimal effect on the CoM and head positions. They suggested a control strategy involving coordinated variations of the major joints to stabilize variables important to postural control during quiet stance. Although the number of degrees of freedom in that study and our study are quite different (six vs. two), in both cases we are faced with a case of redundancy in which a number of solutions are possible for the target posture.

The UCM for the postural control is defined in the joint angle space, while the stable manifold utilized by the proposed intermittent control model is defined in the state space for the model component with no active control. In spite of the difference, we think it makes sense to compare the two approaches, discussing possible relationships between (1) the coordinated joint rotation patterns in postural sway, which are constrained by the UCM, and (2) the sway patterns generated by the off–off model, which are not actively controlled, i.e., are "uncontrolled", when the state of the pendulum is close to the stable manifold of the off–off model. Note that the movement along the stable manifold toward the upright position is energetically "cost free". Since the stable manifold spans a subspace of the state space, dimensionality of the dynamics is reduced if the state of the system is constrained to slide on the stable manifold. More specifically, the stable manifold of the off–off model spans a three dimensional subspace. Thus, the corresponding joint rotation patterns can be restricted to the lower-dimensional joint angle space. This low dimensional space can correspond to the UCM, by which the CoM position is stabilized in a coordinated way on the manifold without active controls. In a similar line of thinking, Bottaro et al. (2005) proposed that the stable manifold of the saddle in the off–off model could be used as a threshold of a sliding mode control (Utkin, 1977), in which the postural state slides along the manifold basically without active control, but with intermittent interventions that pull back the postural state closer to the manifold, leading to chattering-like behaviors in the postural sway. Such behaviors could correspond to the variance of the postural state from the UCM. Detailed analyses are required to elucidate the theoretical relationship between these two types of manifolds defined differently.

The UCM obtained as an averaged movement and motor variations from the UCM can be interpreted in the framework of the theory of optimal feedback control, where the optimal control law is, roughly speaking, determined so that it minimizes the movement-trajectory-dependent global cost referred to as the "cost-to-go" necessary for correcting deviations from the UCM, conditional upon the movement achieves a given task (Todorov, 2004). Such computational mechanism allows redundant movements having null contributions to the cost-to-go and thus can resolve, in principle, dimensionality problem. Regarding postural control, for example, the motor task might be to minimize the oscillations of the CoM around a nominal position. However, even for such a simple task, minimizing the global cost for multi-link body mechanics, with large and variable delays in the feedback loop, might be computationally expensive and functionally inefficient. In this regard, the proposed intermittent control determines the low dimensional manifold, corresponding possibly to the UCM, by the non-actuated body dynamics, and the problems of redundancy and coordination can be resolved by the simple selections of the local-best control alternatives.

6.5. Concluding remarks

We can also view the proposed intermittent control model in the more general framework of the neural control of movements, by considering that goal-oriented movements can be classified into two main sets: discrete and sustained movements (Gawthrop et al., 2011). In the first class there are, for example, reaching movements, which have clear initiation and termination states. In this case, although the final part of these movements can be under continuous feedback control, the basic synergy, which initiates the movements and drives them in the right ball-park, is controlled in open-loop by ballistic motor commands and sequences of well separated discrete movements are under intermittent control by definition. In sustained movements, on the contrary, the neural controller must face either a continuously moving target, as in smooth tracking, or compensate the disturbances of a continuously acting external process/load, like gravity-dependent toppling torques. This is the case, in particular, of upright standing or other tasks involving unstable loads, for which empirical observations of the movements suggest a continuous rather than a discontinuous, intermittent control. However, the stability analysis performed in this paper, which can be generalized from the two-links paradigm to more complex multi-links situations, demonstrates the superiority of a discontinuous, intermittent controller over a conventional continuous controller in terms of robustness to parameter variations, considering the delay in the feedback loop. More specifically, we might be able to apply basically the same state-dependent switching rule for a triple-link and multi-link pendulum, in which CNS controller is required to "know" the stable manifold of the "off model" and to determine a combination of the active joint torques that direct most the stable manifold of the off model.

It is important to clarify that the proposed approach to intermittent control should not be confused with sampled-data or discrete-time control, which became fashionable with the advent of digital computers for the control of industrial processes. In that scheme, the control is constant between samples of sensory information, which are fed to the controller in a discrete manner. In the proposed scheme, on the contrary, sensory information is acquired continuously and the control signals consist of a sequence of (continuous-time) parameterized trajectories whose parameters are adjusted intermittently, according to a state-dependent switching mechanism and not an external clock. As we showed in the paper, from this robust control mechanism, different synergies emerge without any explicit planning but as a consequence of the non-linear dynamics of the decision process when critical parameters of the plant change their values. We believe that this can provide a powerful integrative paradigm for investigating how and when different coordination strategies occur in the multi-link, redundant control of human movements.

Although the multi-segmental posture might be achieved using a set of specific controllers, each dedicated to keep a joint as close as possible to a preplanned angular value (Alexandrov et al., 2005), it has also been proposed that since the goal of postural control is not in terms of configurations of joint angles but in terms of the movements of the projection of the center of mass on the support base, whole body coordination during upright standing may be achieved by many equivalent configurations from which specific cases may be selected according to tasks and environmental conditions (Scholz et al., 2007; Morasso et al., 2010).

Engineering control paradigms, from classical servomechanisms to continuous optimal controllers, suffer the curse of dimensionality and do not scale up well with the degree of redundancy. It is difficult, in such framework, to include in the control loop integrative information as the motion of the center of mass. In contrast, the intermittent framework provides an opportunity to reduce the dimensionality of the problem by introducing lower-dimensionality manifolds that drive the switching on and off of the control signals.

Last but not least, we should remember that, in order to be biologically plausible, a theory of the stabilization strategies of

the human body in the upright posture should incorporate other sensory channels, in addition to proprioceptive information, such as visual, vestibular, light touch, etc. This is clearly beyond the proposed theoretical framework. However, we wish to point out that the robustness of the intermittent controller is mainly determined by the fact that it can well accommodate delayed feedback information. Therefore, we can reasonably expect that adding additional, asynchronous sources of feedback information should not destroy the robustness of the finite state machine that attempts to attract the state of the system to the stable manifold of the mechanical plant.

Acknowledgments

This work was supported in part by JSPS Grants-in-aid 21-416, 23300166, and 23650156, MEXT Global COE Program "*in silico* medicine" at Osaka University, E.U. Grants HUMOUR (FP7-ICT-231724), DARWIN (FP7-ICT-270138), and the Mitsubishi Foundation.

Appendix A. Model definition

$$\mathbf{M}=\begin{pmatrix} I_L+I_{HAT}+m_{HAT}l_L^2+2m_{HAT}l_Lh_{HAT} & I_{HAT}+m_{HAT}l_Lh_{HAT} \\ I_{HAT}+m_{HAT}l_Lh_{HAT} & I_{HAT} \end{pmatrix}$$

$$\mathbf{G}=\begin{pmatrix} -gm_Lh_L-gm_{HAT}l_L-gm_{HAT}h_{HAT} & -gm_{HAT}h_{HAT} \\ -gm_{HAT}h_{HAT} & -gm_{HAT}h_{HAT} \end{pmatrix}$$

where I_L and I_{HAT} represent, respectively, the inertia moment of the lower link around the ankle joint and that of the upper link around the hip joint.

Appendix B. Eigenvalues of the continuous control (DDE) models

We assume the following form as a solution of Eq. (15):

$$(\theta_a(t),\theta_h(t),\omega_a(t),\omega_h(t))^{\mathrm{T}} = e^{\lambda t}(\theta_a([-\Delta,0]),\theta_h([-\Delta,0]),\omega_a([-\Delta,0]),\omega_h([-\Delta,0]))^{\mathrm{T}}.$$

Then we have

$$\lambda e^{\lambda t}\begin{pmatrix} \theta_a([-\Delta,0]) \\ \theta_h([-\Delta,0]) \\ \omega_a([-\Delta,0]) \\ \omega_h([-\Delta,0]) \end{pmatrix} = (e^{\lambda t}\mathbf{A}_{\mathrm{passive}}+e^{\lambda(t-\Delta)}\mathbf{A}^i_{\mathrm{active}})\begin{pmatrix} \theta_a([-\Delta,0]) \\ \theta_h([-\Delta,0]) \\ \omega_a([-\Delta,0]) \\ \omega_h([-\Delta,0]) \end{pmatrix} \tag{B.1}$$

Except for the trivial zero solution for the time interval $[-\Delta,0]$, λ should satisfy the eigenequation Eq. (16), which can be written as the following transcendental equation:

$$\lambda^4+(\alpha_{30}+\alpha_{31}e^{-\lambda\Delta})\lambda^3+(\alpha_{20}+\alpha_{21}e^{-\lambda\Delta}+\alpha_{22}e^{-2\lambda\Delta})\lambda^2 +(\alpha_{10}+\alpha_{11}e^{-\lambda\Delta}+\alpha_{12}e^{-2\lambda\Delta})\lambda+(\alpha_{00}+\alpha_{01}e^{-\lambda\Delta}+\alpha_{02}e^{-2\lambda\Delta})=0 \tag{B.2}$$

where α_{mn} are the constants determined by the parameter values in Tables 2 and 3. There is an infinite number of solutions λ of Eq. (B.2) that determine the stability of each DDE model. We obtained them using the Newton method, and selected the four dominant eigenvalues.

Table 2
Variables and parameters for the double pendulum model.

Symbol	Description	Value/unit
θ_a	Ankle joint angle	— rad
θ_h	Hip joint angle	— rad
ω_a	Ankle angular velocity	— rad/s
ω_h	Hip angular velocity	— rad/s
m_L	Mass of lower link	60×0.35 kg
m_{HAT}	Mass of upper link	60×0.62 kg
l_L	Length of lower link	1.70×0.51 m
l_{HAT}	Length of upper link	1.70×0.45 m
h_L	Distance from distal end to lower link CoM	1.70×0.255 m
h_{HAT}	Distance from distal end to upper link CoM	1.70×0.225 m
h	Height of total CoM for $\theta_h=0$	1.70×0.5618 m

Table 3
Viscoelastic coefficients and PD gains.

Symbol	Description	Value(s)/unit
K_a	Passive elastic coefficient at ankle	$0.8mgh$ N m/rad
B_a	Passive viscosity coefficient at ankle	4.0 N m s/rad
K_h	Passive elastic coefficient at hip	From $0.3mgh$ to $1.0mgh$ N m/rad
B_h	Passive viscosity coefficient at hip	10.0 N m s/rad
P_a	Active proportional gain at ankle	From 0 to $1.0mgh$ N m/rad
D_a	Active derivative gain at ankle	From 0 to 200 N m s/rad
P_h	Active proportional gain at hip	From $0.2mgh$ to $0.6mgh$ N m/rad
D_h	Active derivative gain at hip	From 0 to 50.0 N m s/rad
Δ	Delay in the active feedback loop	0.2 s

Appendix C. Root loci and dynamic modes of the continuous control models

Eigenvalues, the corresponding eigenvectors, and the dynamic modes of the continuous off–off model were obtained using the matrix $\mathbf{A}_{\mathrm{passive}}$ defined in Eq. (11). Those of the other continuous control models were obtained from Eqs. (16) and (B.1). We fixed the active gain parameters as in Eq. (10), and varied the passive hip stiffness continuously in the range of $K_h/mgh\in[0.3,1.0]$. Fig. C1 shows the root loci of the four dominant eigenvalues as a function of K_h for the four continuous models. Branches of the loci in Fig. C1 are colored to represent different types of modes. Blue branches represent the in-phase modes for which θ_a and θ_h coordinates of the corresponding eigenvector have the same signs, and ω_a and ω_h coordinates of the corresponding eigenvector have also the same signs, meaning that the lower and upper links move together like a single pendulum. Red branches represent the anti-phase modes for which θ_a and θ_h coordinates of the corresponding eigenvector have opposite signs, and ω_a and ω_h coordinates of the corresponding eigenvector have also opposite signs, meaning that the lower and upper links move in opposite directions.

Modes of the off–off model (Fig. C1(a)). The blue branch at positive-side represents the unstable in-phase mode, referred to as the mode $M^{\mathrm{u,in}}_{\mathrm{off-off}}$-mon (Fig. 3(a)). The blue branch at negative-side represents the stable in-phase mode, referred to as the mode $M^{\mathrm{s,in}}_{\mathrm{off-off}}$-mon (Fig. 3(b)). The red branches for the pair of complex roots with negative real part represent the stable anti-phase mode, referred to as the mode $M^{\mathrm{s,anti}}_{\mathrm{off-off}}$-osc (Fig. 3(c)). The characteristic frequency of the anti-phase oscillation ranges between 1.2 and 3.0 Hz.

Modes of the on–off model (Fig. C1(b)) and its magnification in (e). For small ($K_h/mgh=0.3$) and medium ($K_h/mgh=0.5$) values of K_h, the blue branches at positive and negative sides represent,

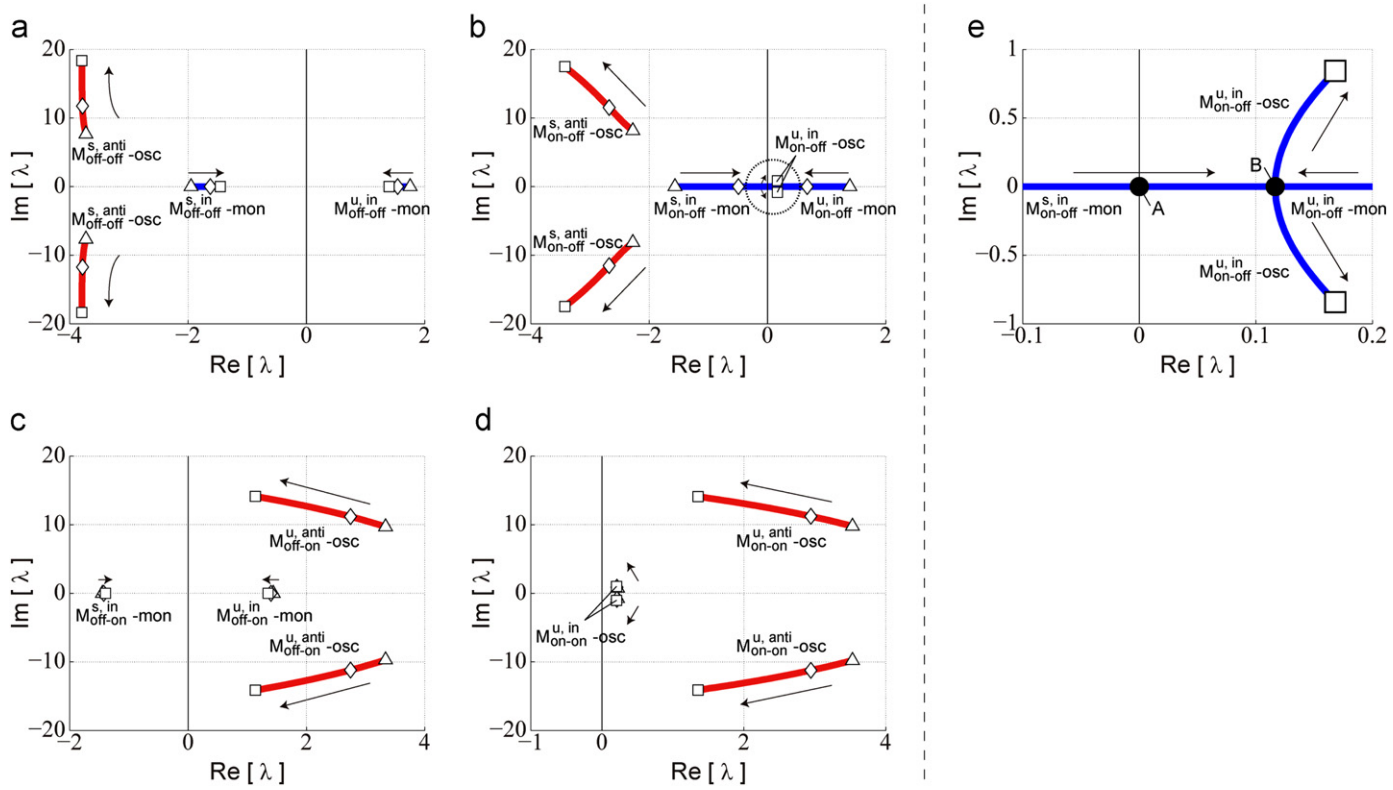

Fig. C1. Root loci of the continuous control models including the off–off model as a function of the passive hip stiffness K_h ($K_a/mgh=0.8$, $B_a=4$ N m s/rad, $P_a/mgh=\{0,0.4\}$, $D_a=\{0,10\}$ N m s/rad, $B_h=10$ N m s/rad, $P_h/mgh=\{0,0.6\}$, $D_h=\{0,10\}$, and $\Delta=0.2$). Panels (a), (b), (c), and (d) are the root loci of the off–off, on–off, off–on, and on–on models, respectively. Each root changes its position along the arrow as K_h increases. Blue and red branches represent the in-phase and the anti-phase modes, respectively. (e) Enlargement of panel (b) around the origin indicated by dotted circle in (b). The point A at the origin is the root for $K_h/mgh=0.5836$. The point B is a bifurcation point of the loci at $K_h/mgh=0.5878$. Markers △, ◇, and □ indicate $K_h/mgh=0.3$, 0.5, and 1.0, respectively.

respectively, the unstable in-phase mode referred to as the $M^{u,in}_{on-off}$-mon (Fig. 3(a)) and the stable in-phase mode referred to as the $M^{s,in}_{on-off}$-mon (Fig. 3(b)). For large K_h ($K_h/mgh=1.0$), the blue branches with complex eigenvalues represent the oscillatory unstable in-phase mode referred to as the $M^{u,in}_{on-off}$-osc (Fig. 3(d)). The red branches with the pair of complex eigenvalues stay at the negative-side for both small and large K_h values. They represent the oscillatory stable anti-phase mode referred to as the $M^{s,anti}_{on-off}$-osc (Fig. 3(c)). The characteristic frequency of the anti-phase oscillatory mode in the on–off model ranges between 1.2 and 2.8 Hz. That of the in-phase oscillatory mode for large K_h is about 0.15 Hz.

Modes of the off–on model (Fig. C1(c)). The blue branches at positive and negative sides represent, respectively, the unstable in-phase mode referred to as the $M^{u,in}_{off-on}$-mon (Fig. 3(a)) and the stable in-phase mode referred to as the $M^{s,in}_{off-on}$-mon (Fig. 3(b)). The remaining two branches colored by red are the pair of complex eigenvalues with positive real part representing the unstable anti-phase mode referred to as the $M^{u,anti}_{off-on}$-osc (Fig. 3(e)). The characteristic frequency of the anti-phase oscillatory mode in the off–on model ranges between 1.5 and 2.3 Hz.

Modes of the on–on model (Fig. C1(d)). There are two pairs of the complex eigenvalues both with positive real parts. One is colored by blue, representing the oscillatory unstable in-phase mode, referred to as the $M^{u,in}_{on-on}$-osc (Fig. 3(d)), and the other by red, representing the oscillatory unstable anti-phase mode referred to as the $M^{u,anti}_{on-on}$-osc (Fig. 3(e)). The characteristic frequency of the anti-phase oscillation in the on–on model ranges between 1.5 and 2.3 Hz. That of the in-phase oscillation is about 0.15 Hz.

Appendix D. The neighborhoods of the stable manifolds

Here we define the neighborhood of the stable manifold of the off–off model and that of the on–off model. The stable manifold of the off–off model is $E^{s,in}_{off-off} \oplus E^{s,anti}_{off-off}$ for any K_h. In the state space E with the coordinate X, a point (x_1,x_2,x_3,x_4) is said to be in the neighborhood of the three-dimensional stable manifold of the off–off model if the following inequality is satisfied.

$$|x_1| \le \alpha^{in}_{off-off}|x_2| \quad \text{and} \quad |x_1| \le \alpha^{anti}_{off-off}\sqrt{x_3^2+x_4^2} \tag{D.1}$$

where $\alpha^{in}_{off-off}$ and $\alpha^{anti}_{off-off}$ are the parameters determining the "thickness" of the neighborhood.

The stable manifold of the on–off model is K_h-dependent. It is $E^{s,in}_{on-off} \oplus E^{s,anti}_{on-off}$ for small and medium K_h, and $E^{s,anti}_{on-off}$ for large K_h. The former is three-dimensional space, and the latter is two-dimensional space. The neighborhood of each of those stable manifolds is defined in the space E represented by the normalized eigenvectors of the corresponding a-ODE model, i.e., the a-on–off model as the basis, just for computational convenience. Note that the sets of basis vectors for the former and the latter are not the same.

For small and medium K_h, a point $(x_1^{on-off},x_2^{on-off},x_3^{on-off},x_4^{on-off})$ is said to be in the neighborhood of the three-dimensional stable manifold $E^{s,in}_{on-off} \oplus E^{s,anti}_{on-off}$ of the on–off model if the following inequality is satisfied:

$$|x_1^{on-off}| \le \alpha^{in}_{on-off}|x_2^{on-off}| \quad \text{and}$$

$$|x_1^{on-off}| \le \alpha^{anti}_{on-off}\sqrt{(x_3^{on-off})^2+(x_4^{on-off})^2} \tag{D.2}$$

where $\alpha^{\mathrm{in}}_{\mathrm{on-off}}$ and $\alpha^{\mathrm{anti}}_{\mathrm{on-off}}$ are the parameters determining the "thickness" of the neighborhood.

For large K_h, a point $(x_1^{\mathrm{on-off}},x_2^{\mathrm{on-off}},x_3^{\mathrm{on-off}},x_4^{\mathrm{on-off}})$ is said to be in the neighborhood of the two-dimensional stable manifold $E^{\mathrm{s,anti}}_{\mathrm{on-off}}$ of the on–off model if the following inequality is satisfied:

$$\sqrt{(x_1^{\mathrm{on-off}})^2+(x_2^{\mathrm{on-off}})^2}\le \alpha^{\mathrm{anti}\prime}_{\mathrm{on-off}}\sqrt{(x_3^{\mathrm{on-off}})^2+(x_4^{\mathrm{on-off}})^2} \tag{D.3}$$

where $\alpha^{\mathrm{anti}\prime}_{\mathrm{on-off}}$ is the parameters determining the "thickness" of the neighborhood.

The parameter values were as follows:

For $K_h/mgh=0.3$: $\alpha^{\mathrm{in}}_{\mathrm{off-off}}=0.3$, $\alpha^{\mathrm{anti}}_{\mathrm{off-off}}=0.03$, $\alpha^{\mathrm{in}}_{\mathrm{on-off}}=0.1$, and $\alpha^{\mathrm{anti}}_{\mathrm{on-off}}=0.07$.

For $K_h/mgh=0.5$: $\alpha^{\mathrm{in}}_{\mathrm{off-off}}=0.4$, $\alpha^{\mathrm{anti}}_{\mathrm{off-off}}=0.01$, $\alpha^{\mathrm{in}}_{\mathrm{on-off}}=0.05$, and $\alpha^{\mathrm{anti}}_{\mathrm{on-off}}=0.1$.

For $K_h/mgh=1.0$: $\alpha^{\mathrm{in}}_{\mathrm{off-off}}=0.6$, $\alpha^{\mathrm{anti}}_{\mathrm{off-off}}=0.01$, and $\alpha^{\mathrm{anti}\prime}_{\mathrm{on-off}}=1$.

Appendix E. Decomposed representation of the physical state

The physical state of the double inverted pendulum at time t, denoted here as $p(t)=(\theta_a(t),\theta_h(t),\omega_a(t),\omega_h(t))$, can be represented using the basis vector (the normalized eigenvector) of the model component that governs the system's dynamics at time t. Note that $p(t)$ is a point in the four-dimensional space E. Note also that $p(t)$ is equivalent with the state point of the intermittent control model $x(t)$ when the system is governed by the off–off model, and it is equivalent with the head $x(t)$ of the state function of the system $x([t-\Delta,t])$ when the system is governed by the i-th DDE model components (i=on–off, off–on, and on–on). The four-dimensional space E can be represented by either Eqs. (12), (18), (20) or Eq. (21) for small and medium K_h, and by either Eqs. (12), (19), (20) or Eq. (21) for large K_h.

When the system is governed by the off–off model component, the manifold-wise power of the physical state of the pendulum at time t is defined as

$$E^{\mathrm{u,in}}_{\mathrm{off-off}}\text{-power}=(p(t),\mathbf{v}_1)^2$$

$$E^{\mathrm{s,in}}_{\mathrm{off-off}}\text{-power}=(p(t),\mathbf{v}_2)^2$$

$$E^{\mathrm{s,anti}}_{\mathrm{off-off}}\text{-power}=(p(t),\mathbf{v}_3)^2+(p(t),\mathbf{v}_4)^2$$

where (a,b) denotes the inner product between two vectors a and b in the standard coordinate. $E^{\mathrm{u,in}}_{\mathrm{off-off}}=\mathrm{span}\{\mathbf{v}_1\}$, $E^{\mathrm{s,in}}_{\mathrm{off-off}}=\mathrm{span}\{\mathbf{v}_2\}$, and $E^{\mathrm{s,anti}}_{\mathrm{off-off}}=\mathrm{span}\{\mathbf{v}_3,\mathbf{v}_4\}$. We say that one (or two) of those three manifolds dominates the dynamics if the corresponding power is clearly larger than the others. The in-phase components (θ_a^{in} and θ_h^{in}) and the anti-phase components (θ_a^{anti} and θ_h^{anti}) of the system's dynamics during the system is governed by the off–off model are defined as follows:

$$\theta_a^{in}(t)=\text{1st row of } (p(t),\mathbf{v}_1)\mathbf{v}_1+(p(t),\mathbf{v}_2)\mathbf{v}_2$$

$$\theta_h^{in}(t)=\text{2nd row of } (p(t),\mathbf{v}_1)\mathbf{v}_1+(p(t),\mathbf{v}_2)\mathbf{v}_2$$

$$\theta_a^{anti}(t)=\text{1st row of } (p(t),\mathbf{v}_3)\mathbf{v}_3+(p(t),\mathbf{v}_4)\mathbf{v}_4$$

$$\theta_h^{anti}(t)=\text{2nd row of } (p(t),\mathbf{v}_3)\mathbf{v}_3+(p(t),\mathbf{v}_4)\mathbf{v}_4$$

When the system is governed by the on–off model component with small and medium K_h, the manifold-wise power of the physical state of the pendulum at time t is defined as follows:

$$E^{\mathrm{u,in}}_{\mathrm{on-off}}\text{-power}=(p(t),\mathbf{v}_1^{\mathrm{on-off}})^2$$

$$E^{\mathrm{s,in}}_{\mathrm{on-off}}\text{-power}=(p(t),\mathbf{v}_2^{\mathrm{on-off}})^2$$

$$E^{\mathrm{s,anti}}_{\mathrm{on-off}}\text{-power}=(p(t),\mathbf{v}_3^{\mathrm{on-off}})^2+(p(t),\mathbf{v}_4^{\mathrm{on-off}})^2$$

$E^{\mathrm{u,in}}_{\mathrm{on-off}}=\mathrm{span}\{\mathbf{v}_1^{\mathrm{on-off}}\}$, $E^{\mathrm{s,in}}_{\mathrm{on-off}}=\mathrm{span}\{\mathbf{v}_2^{\mathrm{on-off}}\}$, and $E^{\mathrm{s,anti}}_{\mathrm{on-off}}=\mathrm{span}\{\mathbf{v}_3^{\mathrm{on-off}},\mathbf{v}_4^{\mathrm{on-off}}\}$. The in-phase and anti-phase components of the system's dynamics during the system is governed by the on–off model are defined as follows:

$$\theta_a^{in}(t)=\text{1st row of } (p(t),\mathbf{v}_1^{\mathrm{on-off}})\mathbf{v}_1^{\mathrm{on-off}}+(p(t),\mathbf{v}_2^{\mathrm{on-off}})\mathbf{v}_2^{\mathrm{on-off}}$$

$$\theta_h^{in}(t)=\text{2nd row of } (p(t),\mathbf{v}_1^{\mathrm{on-off}})\mathbf{v}_1^{\mathrm{on-off}}+(p(t),\mathbf{v}_2^{\mathrm{on-off}})\mathbf{v}_2^{\mathrm{on-off}}$$

$$\theta_a^{anti}(t)=\text{1st row of } (p(t),\mathbf{v}_3^{\mathrm{on-off}})\mathbf{v}_3^{\mathrm{on-off}}+(p(t),\mathbf{v}_4^{\mathrm{on-off}})\mathbf{v}_4^{\mathrm{on-off}}$$

$$\theta_h^{anti}(t)=\text{2nd row of } (p(t),\mathbf{v}_3^{\mathrm{on-off}})\mathbf{v}_3^{\mathrm{on-off}}+(p(t),\mathbf{v}_4^{\mathrm{on-off}})\mathbf{v}_4^{\mathrm{on-off}}$$

Similarly, we can define the manifold-wise powers, the in-phase and the anti-phase components of the physical state of the pendulum at time t for the on–off model component with large K_h, the off–on model component, and the on–on model component.

References

Alexandrov, A., Frolov, A., Horak, F., Carlson-Kuhta, P., Park, S., 2005. Feedback equilibrium control during human standing. Biol. Cybern. 93, 309–322.

Aramaki, Y., Nozaki, D., Masani, K., Sato, T., Nakazawa, K., Yano, H., 2001. Reciprocal angular acceleration of the ankle and hip joints during quiet standing in humans. Exp. Brain Res. 137, 463–473.

Aruin, A., 2002. The organization of anticipatory postural adjustments. J. Autom. Control 12, 31–37.

Asai, Y., Tasaka, Y., Nomura, K., Nomura, T., Casadio, M., Morasso, P., 2009. A model of postural control in quiet standing: robust compensation of delay-induced instability using intermittent activation of feedback control. PLoS ONE 4 (7), art. no. e6169.

Bernstein, N., 1967. The Coordination and Regulation of Movement. Pergamon, London.

Bottaro, A., Casadio, M., Morasso, P., Sanguineti, V., 2005. Body sway during quiet standing: is it the residual chattering of an intermittent stabilization process? Hum. Movement Sci. 24, 588–615.

Bottaro, A., Yasutake, Y., Nomura, T., Casadio, M., Morasso, P., 2008. Bounded stability of the quiet standing posture: an intermittent control model. Hum. Movement Sci. 27, 473–495.

Bouisset, S., Zattara, M., 1987. Biomechanical study of the programming of anticipatory postural adjustments associated with voluntary movement. J. Biomechanics 20, 735–742.

Cabrera, J., Milton, J., 2002. On–off intermittency in a human balancing task. Phys. Rev. Lett. 89, 158702/1–158702/4.

Casadio, M., Morasso, P., Sanguineti, V., 2005. Direct measurement of ankle stiffness during quiet standing: implications for control modelling and clinical application. Gait and Posture 21, 410–424.

Collins, J., De Luca, C., 1993. Open-loop and closed-loop control of posture: a random-walk analysis of center-of-pressure trajectories. Exp. Brain Res. 95, 308–318.

Colobert, B., Crtual, A., Allard, P., Delamarche, P., 2006. Force-plate based computation of ankle and hip strategies from double-inverted pendulum model. Clin. Biomechanics 21, 427–434.

Conforto, S., Schmid, M., Camomilla, V., D'Alessio, T., Cappozzo, A., 2001. Hemodynamics as a possible internal mechanical disturbance to balance. Gait and Posture 14, 28–35.

Creath, R., Kiemel, T., Horak, F., Peterka, R., Jeka, J., 2005. A unified view of quiet and perturbed stance: simultaneous co-existing excitable modes. Neurosci. Lett. 377, 75–80.

Edwards, W., 2007. Effect of joint stiffness on standing stability. Gait and Posture 25, 432–439.

Eurich, C., Milton, J., 1996. Noise-induced transitions in human postural sway. Phys. Rev. E Stat. Phys. Plasmas Fluids Relat. Interdiscip. Top. 54, 6681–6684.

Gawthrop, P., Loram, I., Lakie, M., Gollee, H., 2011. Intermittent control: a computational theory of human control. Biol. Cybern. 104, 31–51.

Horak, F., Nashner, L., 1986. Central programming of postural movements: adaptation to altered support-surface configurations. J. Neurophysiol. 55, 1369–1381.

Horak, F., Nutt, J., Nashner, L., 1992. Postural inflexibility in Parkinsonian subjects. J. Neurol. Sci. 111, 46–58.

Hsu, W.-L., Scholz, J., Schoner, G., Jeka, J., Kiemel, T., 2007. Control and estimation of posture during quiet stance depends on multijoint coordination. J. Neurophysiol. 97, 3024–3035.

Insperger, T., Stepan, G., 2010. On the dimension reduction of systems with feedback delay by act-and-wait control. IMA J. Math. Control Inf. 27, 457–473.

Kaminski, T., 2007. The coupling between upper and lower extremity synergies during whole body reaching. Gait and Posture 26, 256–262.

Kiemel, T., Zhang, Y., Jeka, J., 2011. Identification of neural feedback for upright stance in humans: stabilization rather than sway minimization. J. Neurosci. 31, 15144–15153.

Krishnan, V., Aruin, A., Latash, M., 2011. Two stages and three components of the postural preparation to action. Exp. Brain Res. 212, 47–63.
Loram, I., Lakie, M., 2002a. Direct measurement of human ankle stiffness during quiet standing: the intrinsic mechanical stiffness is insufficient for stability. J. Physiol. 545, 1041–1053.
Loram, I., Lakie, M., 2002b. Human balancing of an inverted pendulum: position control by small, ballistic-like, throw and catch movements. J. Physiol. 540, 1111–1124.
Loram, I., Maganaris, C., Lakie, M., 2004. Paradoxical muscle movement in human standing. J. Physiol. 556, 683–689.
Loram, I., Maganaris, C., Lakie, M., 2005. Human postural sway results from frequent, ballistic bias impulses by soleus and gastrocnemius. J. Physiol. 564, 295–311.
Loram, I., Gollee, H., Lakie, M., Gawthrop, P., 2011. Human control of an inverted pendulum: is continuous control necessary? is intermittent control effective? is intermittent control physiological?. J. Physiol. 589, 307–324.
Manista, G., Ahmed, A., 2012. Stability limits modulate whole-body motor learning. J. Neurophysiol. 107, 1952–1961.
Masani, K., Popovic, M., Nakazawa, K., Kouzaki, M., Nozaki, D., 2003. Importance of body sway velocity information in controlling ankle extensor activities during quiet stance. J. Neurophysiol. 90, 3774–3782.
Maurer, C., Peterka, R., 2005. A new interpretation of spontaneous sway measures based on a simple model of human postural control. J. Neurophysiol. 93, 189–200.
Milton, J., Townsend, J., King, M., Ohira, T., 2009a. Balancing with positive feedback: the case for discontinuous control. Philos. Trans. R. Soc. A Math. Phys. Eng. Sci. Math. 367, 1181–1193.
Milton, J., Ohira, T., Cabrera, J., Fraiser, R., Gyorffy, J., Ruiz, F., Strauss, M., Balch, E., Marin, P., Alexander, J., 2009b. Balancing with vibration: a prelude for "drift and act" balance control. PLoS ONE 4 (10), art. no. e7427.
Morasso, P., 2011. 'Brute force' vs. 'gentle taps' in the control of unstable loads. J. Physiol. 589, 459–460.
Morasso, P., Sanguineti, V., 2002. Ankle muscle stiffness alone cannot stabilize balance during quiet standing. J. Neurophysiol. 88, 2157–2162.
Morasso, P., Spada, G., Capra, R., 1999. Computing the com from the cop in postural sway movements. Hum. Movement Sci. 18, 759–767.
Morasso, P., Casadio, M., Mohan, V., Zenzeri, J., 2010. A neural mechanism of synergy formation for whole body reaching. Biol. Cybern. 102, 45–55.
Nashner, L., McCollum, G., 1985. The organization of human postural movements: a formal basis and experimental synthesis. Behav. Brain Sci. 8, 135–172.
Nomura, K., Fukada, K., Azuma, T., Hamasaki, T., Sakoda, S., Nomura, T., 2009. A quantitative characterization of postural sway during human quiet standing using a thin pressure distribution measurement system. Gait and Posture 29, 654–657.
Peterka, R., 2002. Sensorimotor integration in human postural control. J. Neurophysiol. 88, 1097–1118.
Pinter, I., Van Swigchem, R., Van Soest, A., Rozendaal, L., 2008. The dynamics of postural sway cannot be captured using a one-segment inverted pendulum model: a pca on segment rotations during unperturbed stance. J. Neurophysiol. 100, 3197–3208.
Pozzo, T., Stapley, P., Papaxanthis, C., 2002. Coordination between equilibrium and hand trajectories during whole body pointing movements. Exp. Brain Res. 144, 343–350.
Prieto, T., Myklebust, J., Hoffmann, R., Lovett, E., Myklebust, B., 1996. Measures of postural steadiness: differences between healthy young and elderly adults. IEEE Trans. Biomed. Eng. 43, 956–966.
Priplata, A., Niemi, J., Salen, M., Harry, J., Lipsitz, L., Collins, J., 2002. Noise-enhanced human balance control. Phys. Rev. Lett. 89, 238101/1–238101/4.
Rozendaal, L., Van Soest, A., 2008. Stabilization of a multi-segment model of bipedal standing by local joint control overestimates the required ankle stiffness. Gait and Posture 28, 525–527.
Runge, C., Shupert, C., Horak, F., Zajac, F., 1999. Ankle and hip postural strategies defined by joint torques. Gait and Posture 10, 161–170.
Sasagawa, S., Ushiyama, J., Kouzaki, M., Kanehisa, H., 2009. Effect of the hip motion on the body kinematics in the sagittal plane during human quiet standing. Neurosci. Lett. 450, 27–31.
Schmid, M., Conforto, S., Bibbo, D., D'Alessio, T., 2004. Respiration and postural sway: detection of phase synchronizations and interactions. Hum. Movement Sci. 23, 105–119.
Scholz, J., Schoner, G., 1999. The uncontrolled manifold concept: identifying control variables for a functional task. Exp. Brain Res. 126, 289–306.
Scholz, J., Schoner, G., Hsu, W., Jeka, J., Horak, F., Martin, V., 2007. Motor equivalent control of the center of mass in response to support surface perturbations. Exp. Brain Res. 180, 163–179.
Simpson, D., Kuske, R., Li, Y.-X., 2012. Dynamics of simple balancing models with time-delayed switching feedback control. J. Nonlinear Sci. 22, 135–167.
Stapley, P., Pozzo, T., Cheron, G., Grishin, A., 1999. Does the coordination between posture and movement during human whole-body reaching ensure center of mass stabilization? Exp. Brain Res. 129, 134–146.
Suzuki, Y., Nomura, T., Morraso, P., 2011. Stability of a double inverted pendulum model during human quiet stance with continuous delay feedback control. Proceedings of the Annual International Conference of the IEEE Engineering in Medicine and Biology Society, EMBS, art. no. 6091747, pp. 7450–7453.
Todorov, E., 2004. Optimality principles in sensorimotor control. Nat. Neurosci. 7, 907–915.
Utkin, V.I., 1977. Variable structure systems with sliding modes. IEEE Trans. Autom. Control AC-22, 212–222.
Van Der Kooij, H., De Vlugt, E., 2007. Postural responses evoked by platform perturbations are dominated by continuous feedback. J. Neurophysiol. 98, 730–743.
Vette, A., Masani, K., Nakazawa, K., Popovic, M., 2010. Neural–mechanical feedback control scheme generates physiological ankle torque fluctuation during quiet stance. IEEE Trans. Neural Syst. Rehabil. Eng. 18, 86–95.
Winter, D., Patla, A., Prince, F., Ishac, M., Gielo-perczak, K., 1998. Stiffness control of balance in quiet standing. J. Neurophysiol. 80, 1211–1221.
Yamamoto, T., Suzuki, Y., Nomura, K., Nomura, T., Tanahashi, T., Fukada, K., Endo, T., Sakoda, S., 2011. A classification of postural sway patterns during upright stance in healthy adults and patients with Parkinson's disease. J. Adv. Comput. Intell. Intell. Inf. 15, 997–1010.